

Accepted Manuscript

Shear wave propagation in layered composites with degraded matrices at locations of imperfect bonding

Igor V. Andrianov, Vladyslav V. Danishevskyy, Heiko Topol, Adriaan S. Luyt



PII: S0165-2125(17)30157-9

DOI: <https://doi.org/10.1016/j.wavemoti.2017.12.007>

Reference: WAMOT 2216

To appear in: *Wave Motion*

Received date : 10 July 2017

Revised date : 25 September 2017

Accepted date : 18 December 2017

Please cite this article as: I.V. Andrianov, V.V. Danishevskyy, H. Topol, A.S. Luyt, Shear wave propagation in layered composites with degraded matrices at locations of imperfect bonding, *Wave Motion* (2017), <https://doi.org/10.1016/j.wavemoti.2017.12.007>

This is a PDF file of an unedited manuscript that has been accepted for publication. As a service to our customers we are providing this early version of the manuscript. The manuscript will undergo copyediting, typesetting, and review of the resulting proof before it is published in its final form. Please note that during the production process errors may be discovered which could affect the content, and all legal disclaimers that apply to the journal pertain.

The research highlights of our articles are as follows:

In our article we study biodegradable polymers. These materials find an increasing number of applications in different fields of engineering and medicine due to their environmental-friendly degradation. The process of degradation of biodegradable polymer constituents and the bonding quality between the constituents in composites can be identified by the means of wave propagation through the material together with the analysis of the phononic band structure. In our article we consider a layered composite, in which the matrix degradation is modeled by multiple layers with decreasing values of their mechanical properties.

Bonding between the inclusion and the degrading matrix is taken into account by a linear elastic bonding model in the first case, and by a viscoelastic model in the second case.

Shear wave propagation in layered composites with degraded matrices at locations of imperfect bonding

Igor V. Andrianov^a, Vladyslav V. Danishevskyy^b, Heiko Topol^c, Adriaan S. Luyt^d

^a*Institute of General Mechanics, RWTH Aachen University, Templergraben 64, 52062 Aachen, Germany*

^b*School of Computing and Mathematics, Keele University, Staffordshire, ST5 5BG, UK*

^c*Carnegie Mellon University in Qatar, P.O. Box 24866, Doha, Qatar*

^d*Center for Advanced Materials, Qatar University, P.O. Box 2713, Doha, Qatar*

Abstract

Biodegradable polymers find an increasing number of applications in different fields of engineering and medicine due to their environmental-friendly degradation. The process of degradation of biodegradable polymer constituents and the bonding quality between the constituents in composites can be identified by the analysis of the phononic band structure. The present article considers a layered composite, in which the matrix degradation is modeled by a multitude of layers with decreasing values of their mechanical properties. Bonding between the inclusion and the degrading matrix is taken into account by a linear elastic bonding model in the first case and by a viscoelastic model in the second case.

Keywords: wave propagation, imperfect bonding, biodegradable materials, dispersion relation

1. Introduction

Wave propagation in composites is accompanied by the effects of attenuation and reflection of the propagating signal, which is related to different factors such as the geometry, the mechanical properties of the different constituents, **the prestress of the material [1]**, and the interplay of the different constituents. The analysis of this wave dispersion relation allows drawing conclusions about the influence of the microstructure on **the overall mechanical properties of the composite**, for example, it allows to obtain information about the bonding behavior between the different constituents and the changes in the mechanical properties of certain constituents. **Deformation-independent dispersion relations in a heterogeneous material are studied by Zhang & Parnell [2]**.

In numerous industrial applications, the matrix consists of polymers because of the price, the availability, and the low density of these materials. While these polymers are often non-biodegradable products of the petrochemical industry, nowadays more efforts are made to apply environmental-friendlier biodegradable materials, which can be either natural or even synthetic [3]. Research on

these biodegradable polymers also found an increasing interest, because due to their biodegradable nature these materials are often candidates for different biomedical applications [4]. Different constituents of biological tissues are also natural biodegradable polymers with mechanical properties, which undergo changes due to biochemical or mechanical influences [5]. In the framework of this article we consider an inclusion-matrix composite, in which due to imperfect contact between the constituents the interface between these constituents might be subjected to environmental influences such as air and moisture. We further assume that as a result of air and moisture in this interface the matrix is subjected to degradation and a decline in the mechanical strength. Theories for predicting failures of composite laminates have been reviewed by Icardi et al. [6], and debonding-induced damage in the interface has been studied, for example in the recent article by Safaei et al. [7]. In this article, the degraded matrix region is modeled by multiple layers with increasing or decreasing values of the mechanical properties. A similar approach has been applied by Wu et al. [8], Golub et al. [9], and Fomenko et al. [10] to study the dispersion relation in one-dimensional phononic crystals with functionally graded materials, and by Burla et al. [11] for the determination of effective composite properties.

Wave propagation through a layered composite material and the formation of pass and stop bands is a well-studied topic. Because of relatively simple geometries of layered materials it is often possible to obtain the exact dispersion relation, for example by the application of the Floquet-Bloch approach [12, 13] such as in the articles of Ruzzene & Baz [14] and Shul'ga [15]. A general solution of the dispersion relation for a layered material with an arbitrary number of layers within a periodic unit cell has been presented by Shen & Cao [16]. These exact solutions are useful references to estimate the quality of results, which have been obtained by numerical or semi-analytical methods, for example by the finite difference method [17, 18], by the plane-wave expansion method [19, 20, 21], by Korringa-Kohn-Rostoker method (multiple scattering theory) [22, 23], or by the Rayleigh multipole expansion method [24, 25]. Filonova et al. [26] developed a variant of the computational continua formulation (C^2) in order to study the dispersion relation of layered media, and they use the Floquet-Bloch approach as a reference for their numerical studies. The Floquet-Bloch approach is based in the idealized assumption that the composite is considered to have an infinite length. As discussed by Cao & Qi [27] for a large number of unit cell in a finite structure, the Floquet-Bloch method can provide a reasonable description. In order to study wave propagation in a composite with a finite number of layers, the transfer-matrix method has been applied by different authors [28, 29].

A popular method to study the effective properties of heterogeneous media is the asymptotic homogenization method (AHM), which has been described in detail in the books of Bensoussan et al. [30] and Panasenko [31]. In this approach, the typical size of period of the microstructure is small in comparison to the macroscopic problem, and the ratio of the size of such a period to the region of interest is described by a *small parameter*. Two types coordinate variables are applied, the fast ones, which are related to the size of the heterogeneities, and the slow ones, which are related to the macroscopic size of the considered

problem. By the application of the AHM the original heterogeneous problem can be replaced by a homogeneous material with the same mechanical response, which can simplify the numerical treatment of the material. While the analysis of the material by the Floquet-Bloch approach is often restricted to relatively simple geometries, the AHM gives the possibility to study two-dimensional and three-dimensional problems, more complex geometries of the inclusion [32], and even irregular microstructures [33]. The application of the AHM can be found in different works such as Andrianov et al. [32], Parnell & Abrahams [34], Craster et al. [35, 36], and Antonakakis & Craster [37]. The AHM allows studying nonlinear effects such as geometric, physical, and structural nonlinearity [38]. As pointed out by Andrianov et al. [39], because of the advantages and disadvantages of the different methods to study wave propagation in periodic composites, these methods can be treated mutually complementary. An overview of the AHM of composites can be found in the review by Kalamkarov et al. [40].

We take into account two different types of imperfect bonding: In the first case we apply the spring-layer model, in which the displacements between two neighboring constituents are proportional to the governing stresses at the common interface. This model has been initially proposed by Goland and Reissner [41], and it has found its application in numerous works such as [42, 43, 44]. An alternative model has been presented in the article by Hashin [45], in which imperfect bonding is defined by a thin artificial interphase layer with mechanical properties, which define the bonding quality. Such an interphase model is useful when the mechanical bonding conditions for imperfect bonding cannot be modeled explicitly. *Imperfect bonding between constituents in the asymptotic analysis of composites has been taken into account in the articles of Vivar-Pérez et al. [46] and Andrianov et al. [38].* In the second case we modify the spring-layer model so as to derive viscoelastic bonding characteristics, i.e., the relation between the differences in the displacements of the neighboring constituents at a common interface and the governing stresses at the interface is time-dependent. Examples for articles, in which viscoelastic bonding models have been applied are Gosz et al. [47] and Sadovskii & Chentsov [48]. The mechanical properties of the intact and degraded matrix and the inclusion are considered to be linear elastic. Examples of articles, in which the phononic band structure of composites with viscoelastic properties are studied, are Andrianov et al. [49], Liu et al. [50], and Wang et al. [51].

This article is organized as follows: In Section 2 we introduce the layered problem under consideration, the different bonding models as well as the modeling of the matrix degradation. In Section 3 we consider a layered composite material of infinite length, and we apply the Floquet-Bloch approach in order to obtain exact solutions for the pass and stop bands. Section 4 considers layered composites of finite lengths. The transfer-matrix method is applied in order to study the wave dispersion relation, which results from the location of a single degraded unit cell in the layered material, and the progress of the matrix degradation in this defect cell. In section 5 we apply the asymptotic homogenization method (AHM) in order to determine the macroscopic mechanical properties of the composite, which result from the mechanical and geometric properties

of the microstructure and from the bonding quality between the constituents. This approach allows gaining information about the degradation of the matrix and the decline of the bonding quality by measuring the effective properties of the composite. In the final section we discuss the herein obtained results and draw a brief conclusion.

2. Degraded composite

We study linear shear wave propagation in a layered composite material, which consists of a periodic arrangement of unit cells as shown in Fig. 1. We

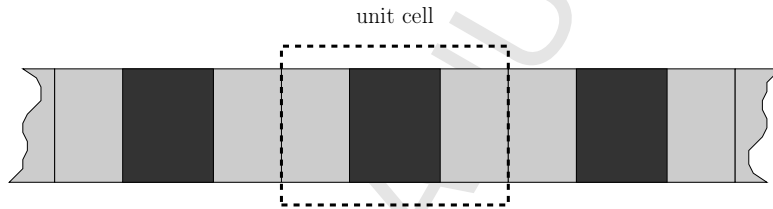


Figure 1: A layered composite material of infinite length, which consists of a periodic arrangement of unit cells.

assume that every unit cell consists of a matrix and an inclusion in its center. Bonding between the matrix and the inclusion might be imperfect. Due to the lack of protection of the matrix at the interface between the matrix and the inclusion from environmental influences such as moisture, we assume that the matrix has degraded at the interface. Such a degradation of the matrix might be a result of corrosion induced by moisture in the imperfect interface. Another example is the degradation of a biodegradable polymer to environmental influences. Examples of such a system are biodegradable polymers like poly(lactic acid) (PLA) reinforced with organic fillers, or blended immiscibly with another polymer, where the other polymer is the minor phase, which will form spherical inclusions in the PLA matrix.

2.1. Arrangements and mechanical properties of the constituents

A single unit cell of the composite material in Fig. 1 is illustrated in Fig. 2. The top part of Fig. 2 shows such a unit cell of $2N - 1$ layers $\Omega^{(n)}$, which are in symmetric arrangement. The layer $\Omega^{(n)}$, where $n = 1, 2, \dots, N$, has a shear modulus $\mu^{(n)}$, a mass density $\rho^{(n)}$, and a total length $\ell^{(n)}$. We apply the notation $\Omega_{\pm}^{(n)}$, in which the subscript " \pm " describes the location of a layer within a unit cell: the notation $\Omega_{-}^{(n)}$ indicates that the layer is located on the left side of the unit cell, and the notation $\Omega_{+}^{(n)}$ indicates that the layer is located on the right side of the unit cell. The layer $\Omega_{\pm}^{(1)} = \Omega^{(1)}$ in the center of a unit cell is the inclusion. All further layers $\Omega_{\pm}^{(2)}, \Omega_{\pm}^{(3)}, \dots, \Omega_{\pm}^{(N)}$ represent the matrix.

We assume that bonding between the inclusion $\Omega^{(1)}$ and the neighboring matrix layers $\Omega_{\pm}^{(2)}$ at the common interface $\partial\Omega_{\pm}^{(1,2)}$ might be imperfect. Such

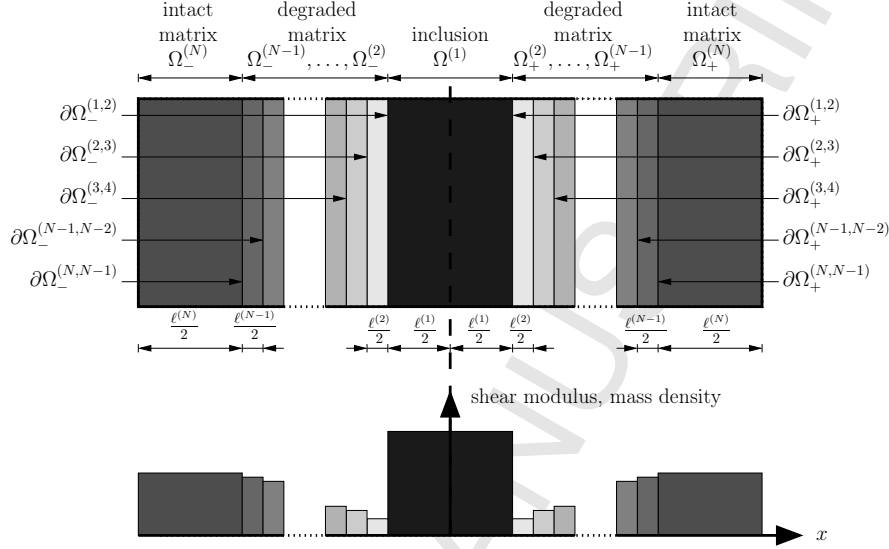


Figure 2: A single unit cell of a periodic composite in Fig. 1.

an imperfect bonding might be, for example, the result of insufficient adherence between the components due to a production error, or it might be the result of a crack due to weak or no interfacial interaction between the matrix polymer and the inclusions. Due to the lack of protection of the matrix at the interface $\partial\Omega_{\pm}^{(1,2)}$ from environmental influences, we assume that the matrix has degraded at the interface. This degraded part of the matrix is simulated by the $N - 2$ layers $\Omega_{\pm}^{(2)}, \Omega_{\pm}^{(3)}, \dots, \Omega_{\pm}^{(N-1)}$. The outer layers of the unit cell $\Omega_{\pm}^{(N)}$ shall represent the intact part of the matrix. The higher the number of layers, which simulate the degraded part of the matrix, the better is the accuracy of the proposed model. A similar approach has been applied by Wu et al. [8], Golub et al. [9], and Fomenko et al. [10] in order to model functionally graded materials.

We consider linear shear wave propagation into the direction x through the composite, which is described by the wave equation

$$\mu^{(n)} \frac{\partial^2 u_{\pm}^{(n)}}{\partial x^2} = \rho^{(n)} \frac{\partial^2 u_{\pm}^{(n)}}{\partial t^2}, \quad n = 1, 2, \dots, N, \quad (1)$$

where $u_{\pm}^{(n)} = u_{\pm}^{(n)}(x, t)$ is the displacement perpendicular to the direction of propagation x at time t in the layer $\Omega_{\pm}^{(n)}$.

2.2. Bonding models

2.2.1. Elastic Bonding Models

The interplay of the different constituents has a strong impact on the macroscopic mechanical behavior of the composite. The matrix layers $\Omega_{\pm}^{(n)}$ and $\Omega_{\pm}^{(n+1)}$ for $n = 2, 3, \dots, N - 1$ are assumed to be in perfect contact at their common

interface $\partial\Omega_{\pm}^{(n,n+1)}$, so that the displacements as well as the shear stresses are considered to be equal at this interface,

$$u_{\pm}^{(n)} \Big|_{\partial\Omega_{\pm}^{(n,n+1)}} = u_{\pm}^{(n+1)} \Big|_{\partial\Omega_{\pm}^{(n,n+1)}}, \quad (2a)$$

$$\mu^{(n)} \frac{\partial u_{\pm}^{(n)}}{\partial x} \Big|_{\partial\Omega_{\pm}^{(n,n+1)}} = \mu^{(n+1)} \frac{\partial u_{\pm}^{(n+1)}}{\partial x} \Big|_{\partial\Omega_{\pm}^{(n,n+1)}}. \quad (2b)$$

Let us now assume that bonding between the inclusion $\Omega^{(1)}$ and the neighboring matrix layer $\Omega_{\pm}^{(2)}$ at their common interfaces $\partial\Omega_{\pm}^{(1,2)}$ might be imperfect, and that difference in the displacements at this interface is proportional to the governing shear stress:

$$\pm [u_{\pm}^{(2)} - u_{\pm}^{(1)}]_{\partial\Omega_{\pm}^{(1,2)}} = \mu^{(1)} \frac{\partial u^{(1)}}{\partial x} \Big|_{\partial\Omega_{\pm}^{(1,2)}} \gamma^{(1,2)}, \quad (3a)$$

$$\mu^{(1)} \frac{\partial u^{(1)}}{\partial x} \Big|_{\partial\Omega_{\pm}^{(1,2)}} = \mu^{(2)} \frac{\partial u_{\pm}^{(2)}}{\partial x} \Big|_{\partial\Omega_{\pm}^{(1,2)}}. \quad (3b)$$

The upper sign in \pm refers to interfaces $\partial\Omega_{+}^{(n,n+1)}$ on the right side of the unit cell in Fig. 2, and the bottom sign to the interfaces $\partial\Omega_{-}^{(n,n+1)}$ on the left side of the unit cell. In order to quantify the bonding quality between $\Omega_{\pm}^{(n)}$ and $\Omega_{\pm}^{(n+1)}$ by a single parameter, we introduce the bonding factor $\gamma^{(n,n+1)}$, which we want to define as

$$\frac{\ell^{(if)}}{\mu^{(if)}} = \gamma^{(1,2)}. \quad (4)$$

Here a modeling interphase layer $\Omega^{(if)}$ with a length $\ell^{(if)} \rightarrow 0$ and a shear modulus $\mu^{(if)}$ is introduced, and the properties of such an interphase describe the bonding quality between the layers $\Omega^{(1)}$ and $\Omega_{\pm}^{(2)}$ at the common interface $\partial\Omega_{\pm}^{(1,2)}$. The details of this model are derived in Appendix A. Due to the analogy to **the mechanical behavior** of a linear spring, such a model is denoted as a *spring-layer model* (see left part of Fig. 3). This spring-layer model has been proposed by Goland & Reissner [41], and it has been applied in different studies such as [43, 44].

If we take the mechanical properties of the modeling interphase $\Omega^{(if)}$ to be elastic, then the shear modulus $\mu^{(if)}$ of $\Omega^{(if)}$ and consequently the bonding factor $\gamma^{(1,2)}$ in (4) are constants. Although the herein considered spring-layer model has been derived in order to model a mechanical imperfect interface, it is worth to mention that this model shows analogies to the Kapiza interface model [52], which has been developed in order to model for thermal resistance between constituents at common interfaces. Analogously to the here presented procedure to derive such linear bonding model, this model can be extended to describe a nonlinear imperfect interface. Examples of works that model



Figure 3: Two bonding models: The elastic spring-layer model can be simulated by a spring. In order to model viscoelastic behavior, bonding between two constituents at their common interface is simulated by a Kelvin-Voigt element, which consists of spring and a dashpot in parallel arrangement.

nonlinear imperfect interfaces are the articles by Levi & Dong [53], Levi [54], Andrianov et al. [38] and Danishevskyy et al. [55]. A similar approach to model nonlinear thermal resistance can be found in [56, 57].

2.2.2. Viscoelastic bonding model

We seek to modify the bonding model to take into account viscoelastic behavior, so that the bonding quality depends on the frequency ω of the traveling signal. This bonding quality is described by the bonding factor $\gamma^{(1,2)}$ in (4), which is defined by the ratio of the length $\ell^{(if)}$ to the shear modulus $\mu^{(if)}$ of the modeling material. If we take the shear modulus in the modeling interphase $\Omega^{(if)}$ to be viscoelastic, then $\mu^{(if)} = \mu^{(if)}(\omega)$ becomes a function of the frequency ω of the propagating wave. We want to model the mechanical behavior of $\mu^{(if)}(\omega)$ in terms of the Kelvin-Voigt model, in which the bonding behavior is described by a spring in parallel arrangement to a dashpot as shown in the right part of Fig. 3. The spring represents the elastic behavior of the interface, and the dashpot represents the viscous character of the interface so that

$$\mu^{(if)}(\omega) = \mu_R^{(if)} + i\mu_I^{(if)}(\omega), \quad (5a)$$

$$\mu_I^{(if)}(\omega) = \nu^{(if)}\omega, \quad (5b)$$

where $i = \sqrt{-1}$. The bonding factor $\gamma^{(1,2)} = \gamma^{(1,2)}(\omega)$ in (4) then also becomes a complex and frequency dependent function in the form

$$\gamma^{(1,2)}(\omega) = \frac{\ell^{(if)}}{\mu^{(if)}(\omega)} = \frac{\ell^{(if)}}{\mu_R^{(if)} + i\mu_I^{(if)}(\omega)} = \frac{\ell^{(if)}}{\mu_R^{(if)} + i\nu^{(if)}\omega}. \quad (6)$$

Examples of works that studied viscoelastic interfaces models are Gosz et al. [47] and Sadovskii & Chentsov [48]. The opposite case of the here treated problem, in which the constituents are taken to be viscoelastic and the bonding model to reveal elastic behavior, has been studied in the recent article by Andrianov et al. [49].

It might be difficult to model imperfect bonding between the constituents explicitly by the boundary conditions at a common interface between the constituents. One technique to overcome this problem is by introducing an artificial interphase layer with geometric and mechanical properties, which define the bonding quality (see, for example, Hashin [45]). One disadvantage of the

interphase layer approach is that introducing an artificial layer slightly changes the geometry of the overall problem. The article [49] compares the interphase layer approach to an approach, in which imperfect bonding is directly described by boundary conditions in the interface in a layered material, by the application of the Floquet-Bloch method. Contrasting both approaches allows to estimate and minimize the error in the interphase layer approach, before such a model is applied in further studies.

3. Exact solution for the dispersion relation for an infinite number of unit cells: Floquet-Bloch approach

We consider shear wave propagation in a direction x through a layered composite material. Such a composite is shown in Fig. 1, and we take the composite to be composed of an infinite number of equal unit cells of length ℓ . Each unit cell consists of N layers $\Omega_{\pm}^{(n)}$ with a thickness $\ell^{(n)}$, a constant shear modulus $\mu^{(n)}$, and a constant mass density $\rho^{(n)}$, where $n = 1, 2, \dots, N$ and $\sum_{n=1}^N \ell^{(n)} = \ell$.

The Floquet-Bloch approach allows obtaining exact results for such relatively simple and idealized geometries. In order to study the frequency band formation of the composite, we consider propagation of a Floquet-Bloch shear wave [13, 12] as a superposition of waves traveling into the positive and into the negative x -direction, respectively, in the form

$$u_{\pm}^{(n)}(x, t) = U_{\pm}^{(n)}(x) \exp(ikx) \exp(i\omega t) \quad (7)$$

for x located in $\Omega_{\pm}^{(n)}$, where ω is the frequency of the traveling signal, and

$$k = k_R + ik_I \quad (8)$$

is the complex effective wavenumber of the composite with the real part k_R and the imaginary part k_I . By rewriting the exponential term $\exp(ikx) = \exp(ik_R x) \exp(-k_I x)$ in (7), it can be shown that the traveling wave attenuates exponentially with the imaginary part of the wavenumber k_I , which is also denoted as the attenuation coefficient. In (7), $U_{\pm}^{(n)}(x)$ is a spatially periodic function, which takes the influence of the microstructure into account,

$$U_{\pm}^{(n)}(x) = U_{\pm}^{(n)}(x + \ell), \quad (9)$$

where also for $U_{\pm}^{(n)}(x)$ the subscript \pm indicates the location of $\Omega_{\pm}^{(n)}$ in the unit cell,

$$U_{\pm}^{(1)}(x) = U^{(1)}(x), \quad (10a)$$

$$U_{\pm}^{(n)}(x) = \begin{cases} U_{+}^{(n)}(x) & \text{if } x > 0, \quad n = 2, 3, \dots, N, \\ U_{-}^{(n)}(x) & \text{if } x < 0, \quad n = 2, 3, \dots, N. \end{cases} \quad (10b)$$

Equation (10a) is for the inclusion, and (10b) for the different matrix layers. By substituting (9) into (7), we can directly show that the displacements at the outer boundaries of the unit cell are related by the condition

$$u_+^{(N)}(x + \ell, t) = u_-^{(n)}(x, t) \exp(ik\ell). \quad (11)$$

After substitution of the Floquet-Bloch ansatz (7) into the wave Eq. (1), we obtain the periodic function (9) in terms of $U_{1,\pm}^{(n)}$ and $U_{2,\pm}^{(n)}$,

$$U_{\pm}^{(n)}(x) = U_{1,\pm}^{(n)} \exp\left(i \left[k^{(n)} - k\right] x\right) + U_{2,\pm}^{(n)} \exp\left(-i \left[k^{(n)} + k\right] x\right), \quad (12)$$

where

$$k^{(n)} = \omega \sqrt{\frac{\rho^{(n)}}{\mu^{(n)}}} \quad (13)$$

are the wavenumbers of the constituents $\Omega_{\pm}^{(n)}$. On the right side of Eq. (12), $U_{1,\pm}^{(1)}$ are the amplitudes of the waves traveling into the positive x -direction, $U_{2,\pm}^{(1)}$ are the amplitudes of the waves traveling into the negative x -direction:

$$\{U_{1,\pm}^{(1)}, U_{2,\pm}^{(1)}\} = \{U_1^{(1)}, U_2^{(1)}\}, \quad (14a)$$

$$\{U_{1,\pm}^{(n)}, U_{2,\pm}^{(n)}\} = \begin{cases} \{U_{1,+}^{(n)}, U_{2,+}^{(n)}\} & \text{if } x > 0, \quad n = 2, 3, \dots, N \\ \{U_{1,-}^{(n)}, U_{2,-}^{(n)}\} & \text{if } x < 0, \quad n = 2, 3, \dots, N. \end{cases} \quad (14b)$$

After combining Eqs. (7) and (12), we obtain the displacement function for each layer in the form

$$u_{\pm}^{(n)}(x, t) = \left[U_{1,\pm}^{(n)} \exp\left(ik^{(n)}x\right) + U_{2,\pm}^{(n)} \exp\left(-ik^{(n)}x\right) \right] \exp(i\omega t). \quad (15)$$

Section 2.2 has introduced the boundary conditions for both perfect bonding between all interfaces within the matrix, and for imperfect bonding applicable to **both** interfaces between the inclusion $\Omega^{(1)}$ and the neighboring matrix layers $\Omega_{\pm}^{(2)}$. Recalling condition (11), which results from the periodicity of the microstructure, and assuming perfect contact between a unit cell **and its two** neighboring unit cells, the displacements and shear stresses at the outer unit cell interfaces at $x = \pm \frac{\ell}{2}$ are related via

$$u_+^{(N)} \Big|_{x=\frac{\ell}{2}} = u_-^{(N)} \Big|_{x=-\frac{\ell}{2}} \exp(ik\ell), \quad (16a)$$

$$\mu^{(N)} \frac{\partial u_+^{(n)}}{\partial x} \Big|_{x=\frac{\ell}{2}} = \mu^{(N)} \frac{\partial u_-^{(n+1)}}{\partial x} \Big|_{x=-\frac{\ell}{2}} \exp(ik\ell). \quad (16b)$$

The conjugate conditions (2), (3), and (16) give a linear system of $2N - 1$ equations of the unknown parameters $U_{1,\pm}^{(n)}$ and $U_{2,\pm}^{(n)}$. The non-trivial solution

of the determinant of the matrix of these parameters $U_{1,\pm}^{(n)}$ and $U_{2,\pm}^{(n)}$ gives an exact solution to the relation between the wavenumber k and the frequency ω of the propagating wave (see Appendix B). The results for the real part k_R of the wavenumber for the frequency ω intervals are denoted as pass bands, where wave propagation is possible. The results for the imaginary part k_I of the wavenumber for the frequency ω intervals are denoted as stop bands, in which the traveling signal attenuates exponentially.

In the following examples, the Floquet-Bloch method is applied to illustrate the effect of matrix degradation on dispersion relation of the composite.

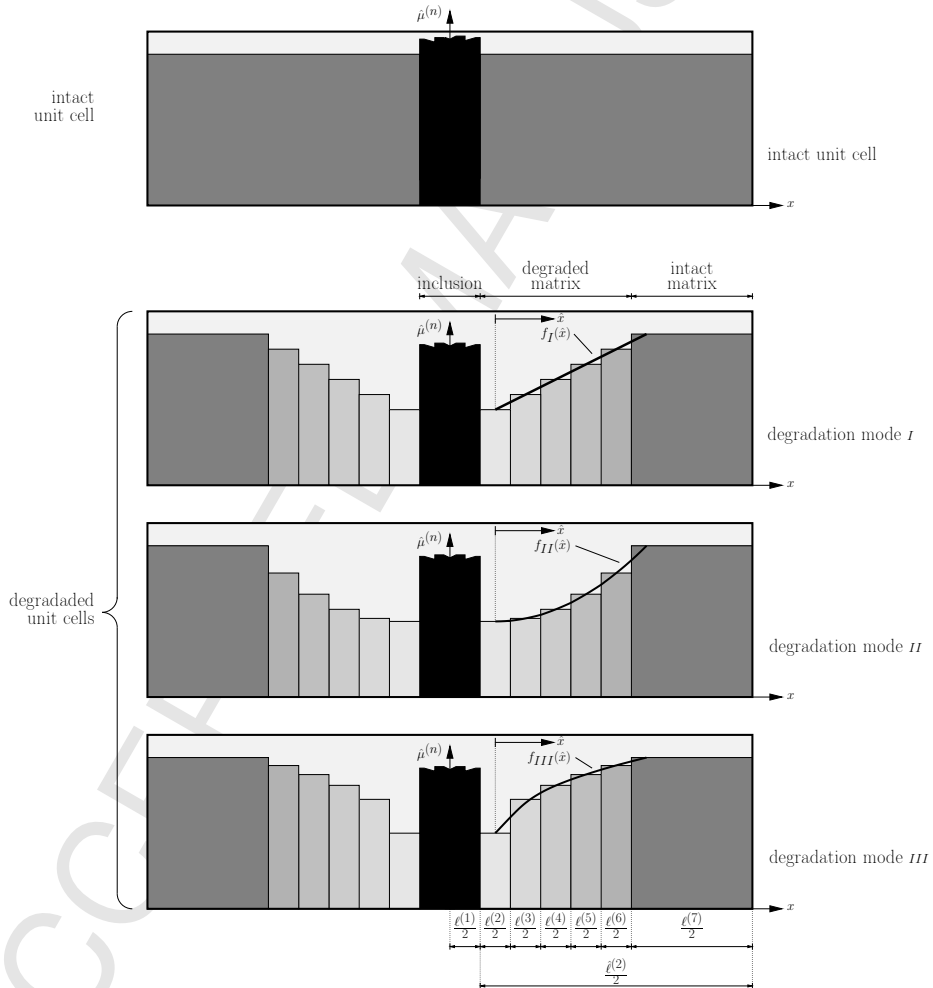


Figure 4: Distribution of the material parameters in an intact unit cell and in unit cells with degraded matrices. For the degradation, we take into account three degradation modes of the matrix, which are described by the three functions (17).

3.1. Numerical examples: infinite layer of unit cells with degraded matrices

Consider a layered composite as illustrated in Fig. 2, which consists of the inclusion layer $\Omega^{(1)}$ with the length $\ell^{(1)} = \frac{\ell}{10}$, and a matrix, which in turn is modeled by six layers $\Omega_{\pm}^{(2)}, \Omega_{\pm}^{(3)}, \dots, \Omega_{\pm}^{(7)}$. The layers $\Omega_{\pm}^{(2)}, \Omega_{\pm}^{(3)}, \dots, \Omega_{\pm}^{(6)}$ shall simulate the degraded part of the matrix, and each of these layers is assumed to have a total length of $\ell^{(2)} = \ell^{(3)} = \dots = \ell^{(6)} = \frac{\ell}{10}$, while the intact part of the matrix $\Omega_{\pm}^{(7)}$ has a total length of $\ell^{(7)} = \frac{\ell}{4}$. A crack might have occurred at the interface $\partial\Omega^{(1,2)}$, and the matrix starts to degrade from this interface. In Fig. 4 we depict three different degradation modes, which are described by the three functions

$$\text{degradation mode I : } f_I(\hat{x}) = a_I \hat{x} + b_I, \quad (17a)$$

$$\text{degradation mode II : } f_{II}(\hat{x}) = a_{II} \hat{x}^2 + b_{II}, \quad (17b)$$

$$\text{degradation mode III : } f_{III}(\hat{x}) = a_{III} \sqrt{\hat{x}} + b_{III}, \quad (17c)$$

where a_I, a_{II}, a_{III} and b_I, b_{II}, b_{III} are positive constants. These constants are chosen in order to quantify the degradation process of the matrix. The first degradation mode in (17a) describes degradation, which is proportional to the distance from the inclusion. The second degradation mode in (17b) describes degradation, which is proportional to the square of the distance from the inclusion. The third degradation mode in (17c) describes degradation, which is proportional to the square root of the distance from the inclusion.

For the inclusions we apply the material parameters of aluminum (shear modulus $\mu^{(1)} = 26$ GPa, mass density $\rho^{(1)} = 2700$ kg/m³), and for the intact part of the matrix we apply the material parameters of poly(lactic acid) (PLA) (shear modulus $\mu^{(10)} = 1.287$ GPa, mass density $\rho^{(10)} = 1251.5$ kg/m³ [58]).

The following part of the present section is now subdivided into three paragraphs, in which three different problems are studied:

- In the first example we consider linear matrix degradation as described by (17a), starting from the inclusion-matrix interface $\partial\Omega_{\pm}^{(1,2)}$, and we study how ongoing matrix degradation changes the frequency band formation.
- In the second example, we contrast the differences in the frequency band formation for the three degradation modes in Eqs. (17), which are illustrated in Fig. 4.
- In the first and second part, we assume that bonding between the inclusion and the matrix $\partial\Omega_{\pm}^{(1,2)}$ is perfect. In the last part of the examples, we study the impact of the different viscoelastic bonding models on the wave attenuation for a matrix, which has been degraded linearly.

In all the examples the inclusion $\Omega^{(1)}$ is assumed to not to be affected by the degradation of the matrix.

3.1.1. Linear Matrix Degradation

In the first part of the numerical examples, we consider a process of linear degradation of the matrix, starting from the inclusion-matrix interface $\partial\Omega_{\pm}^{(1,2)}$ as it is depicted in Fig. 4 for degradation mode I . Table 1 shows the different

shear moduli of the matrix						
	$\hat{\mu}^{(2)}$	$\hat{\mu}^{(3)}$	$\hat{\mu}^{(4)}$	$\hat{\mu}^{(5)}$	$\hat{\mu}^{(6)}$	$\hat{\mu}^{(7)}$
lin 0	1	1	1	1	1	1
lin 1	0.9	1	1	1	1	1
lin 2	0.8	0.9	1	1	1	1
lin 3	0.7	0.8	0.9	1	1	1
lin 4	0.6	0.7	0.8	0.9	1	1
lin 5	0.5	0.6	0.7	0.8	0.9	1

Table 1: Linear degradation of the matrix as illustrated in the top part of Fig. 4.

values of the material parameters of the matrix, where

$$\hat{\mu}^{(n)} = \frac{\mu^{(n)}}{\mu^{(7)}} = \frac{\rho^{(n)}}{\rho^{(7)}}, \quad n = 2, 3, \dots, 7. \quad (18)$$

In (18) we assume that the decline of the mass density of the degraded material is proportional to the decline of the shear modulus during the degradation process. The gray cells in Tab. 1 illustrate the values of the degraded material, while the white cells represent the intact part of the matrix. In the present example we assume perfect bonding between all the neighboring layers. The results for the frequency bands are presented in Fig. 5, where $\bar{k} = k\ell$ is the normalized effective wavenumber and $\bar{\omega} = \omega\ell\sqrt{\frac{\rho^{(1)}}{\mu^{(1)}}}$ is the normalized frequency. The curves in the white areas are the pass bands that illustrate the relation between the real part of the wavenumber and the frequency. The curves in the gray areas are the stop bands, which illustrate the relation between the imaginary part of the wavenumber and the frequency. Figure 5 (a) shows the band formation for a composite with an intact matrix. The next panels "lin m ", where $m = 1, 2, 3, 4, 5$, illustrate the shift of these bands with the number of layers, which are affected by the linear degradation process. In all the panels the results for the degraded materials are plotted as solid lines, while the results for the intact matrix are plotted as dashed lines.

The different panels illustrate that for the herein chosen material parameters and linear degradation model, the boundaries of the frequency bands shift with the degradation process of the matrix. For example, the first stop band becomes narrower with ongoing matrix degradation, while the following stop bands become larger on the herein considered frequency range. **This effect is explained as follows: The change of the matrix material parameters with the degradation process has an impact on the boundary conditions in (2). The non-trivial**

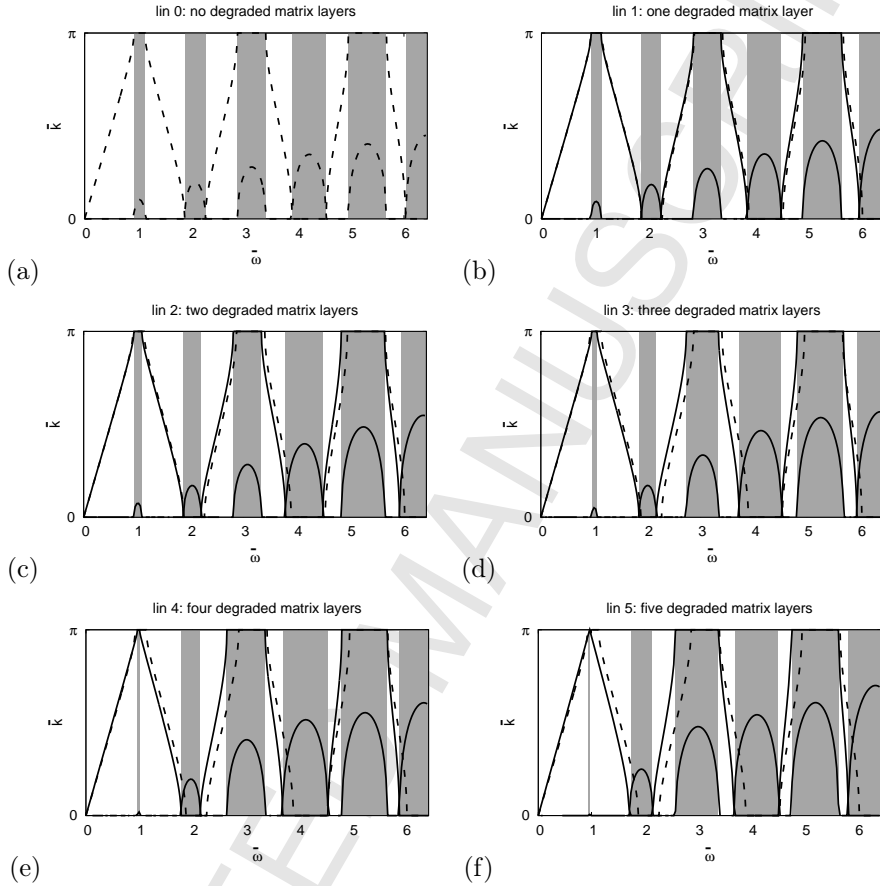


Figure 5: Frequency bands for the materials in Tab. 1, where $\bar{k} = k\ell$ is the normalized wavenumber and $\bar{\omega} = \omega\ell\sqrt{\rho^{(1)}/\mu^{(1)}}$ is the normalized frequency.

solution of the determinant of the matrix (see Appendix B) of the parameters $U_{1,\pm}^{(n)}$ and $U_{2,\pm}^{(n)}$ in (14) changes at any instant of the degradation process, which results into an evolving relation between the wavenumber and the frequency.

3.1.2. Three different degradation modes

In the previous example, we studied the development of the frequency band structure with ongoing linear degradation of the matrix, as depicted in Fig. 4 for degradation mode *I*. The most advanced matrix degradation has been considered in Fig. 5 (g), where five matrix layers have been degraded.

Let us now compare this frequency band structure in Fig. 5 (g) for degradation mode *I* to the degradation modes *II* and *III*, which are also depicted in Fig. 4. These three degradation modes are described by the functions $f_I(\hat{x})$, $f_{II}(\hat{x})$, and $f_{III}(\hat{x})$ in Eqs. (17), where the different parameters $a_I = 2\ell^{-1}$,

	shear moduli of the matrix						
degradation mode	$\hat{\mu}^{(2)}$	$\hat{\mu}^{(3)}$	$\hat{\mu}^{(4)}$	$\hat{\mu}^{(5)}$	$\hat{\mu}^{(6)}$	$\hat{\mu}^{(7)}$	Eq.
<i>I</i>	0.5000	0.6000	0.7000	0.8000	0.9000	1.000	(17a)
<i>II</i>	0.5000	0.5200	0.5800	0.6800	0.8200	1.000	(17b)
<i>III</i>	0.5000	0.7236	0.8162	0.8873	0.9471	1.000	(17c)

Table 2: Linear degradation of the matrix. The table shows the different values for $\hat{\mu}^{(n)} = \frac{\mu^{(n)}}{\mu^{(10)}}$, where $n = 2, 3, \dots, 10$. The values of the degraded cells are highlighted.

$a_{II} = 8 \ell^{-2}$, $a_{III} = \ell^{-\frac{1}{2}}$, and $b_I = b_{II} = b_{III} = 0.5$ are chosen in a way that the first degraded matrix layers $\Omega_{\pm}^{(2)}$ have the same material parameters for the three degradation modes. In all three cases, the matrix has the same length $\frac{4}{10} \ell$. The material parameters of the matrix are given in Tab. 2 for the three degradation modes.

The results for the frequency band formations of all three degradation modes are depicted in Fig. 6. As a reference, the frequency bands for the composite with the intact matrix are also presented. Figure 6 (a) contrasts the results for the pass bands, and Fig. 6 (b) the results for the stop bands.

The different degradation modes result into frequency bands, which differ in the location and magnitude. All second, third, ..., and sixth local maxima in Fig. 6 (b) are larger for the degraded matrices in comparison to the maxima for the intact matrix. If we compare the results for the different degradation modes, then we find that the differences in the local maxima are relatively large for the second and third stop bands, and relatively small for the then following stop bands. Each dispersion relation can be seen as a "fingerprint" for composition of the composite, and the mechanical properties of the different constituents. Studying the frequency band formation allows to draw conclusions about the microstructure of the material and to describe the progress in the matrix damage. An example is the article of Hussein et al. [59], in which the authors conclude the composition of a layered composite for a given dispersion relation.

3.1.3. Imperfect bonding between the inclusion and the matrix

In order to study the impact of the bonding quality between the inclusion $\Omega^{(1)}$ and the matrix $\Omega^{(2)}$ at the common interface $\partial\Omega^{(1,2)}$, let us consider an intact matrix. In Sect. 2.2 we introduced a model for imperfect bonding, in which the bonding quality is defined by a single parameter, the bonding factor $\gamma^{(1,2)}$. This parameter $\gamma^{(1,2)}$ can be interpreted as the ratio of the length $\ell^{(if)}$ to the shear modulus $\mu^{(if)}$ of an artificial modeling layer, where we assume $\ell^{(if)} \rightarrow 0$. Let us rewrite this bonding factor in the complex form

$$\gamma^{(1,2)}(\omega) = \gamma_R^{(1,2)}(\omega) + i\gamma_I^{(1,2)}(\omega), \quad (19)$$

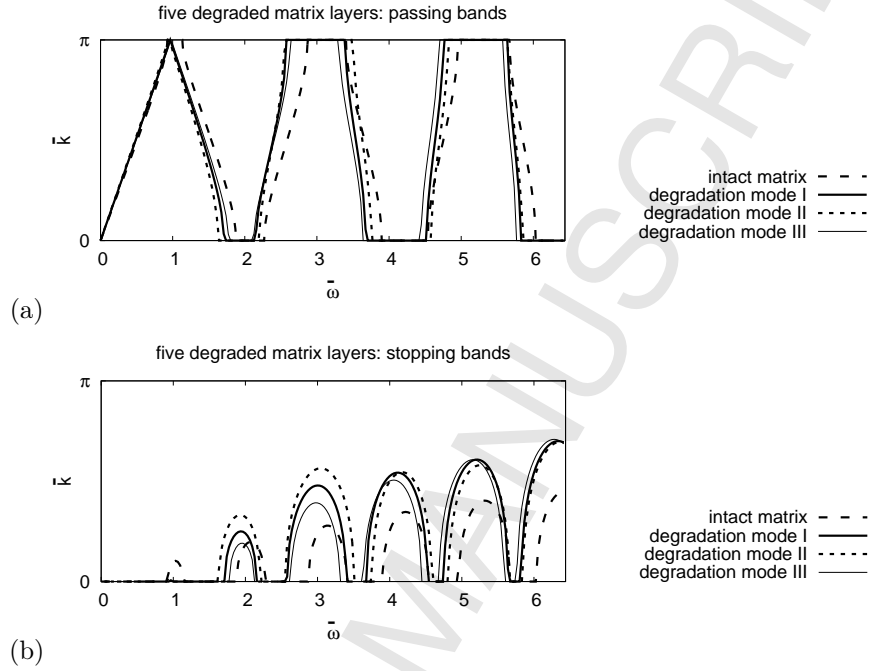


Figure 6: Frequency bands for a layered composite for three different degradation modes, which are presented in Fig. 4.

where both the real part $\gamma_R^{(1,2)} = \gamma_R^{(1,2)}(\omega)$ and the imaginary part $\gamma_I^{(1,2)} = \gamma_I^{(1,2)}(\omega)$ are frequency dependent functions:

$$\gamma_R^{(1,2)}(\omega) = \frac{\ell^{(if)} \mu_R^{(if)}}{[\mu_R^{(if)}]^2 + [\nu^{(if)} \omega]^2}, \quad (20a)$$

$$\gamma_I^{(1,2)}(\omega) = -\frac{\ell^{(if)} \nu^{(if)} \omega}{[\mu_R^{(if)}]^2 + [\nu^{(if)} \omega]^2}. \quad (20b)$$

These forms of the real and imaginary part of the bonding factor in (20) result from the parallel arrangement of the dashpot and the spring as shown in the right part of Fig. 3. This bonding factor $\gamma^{(1,2)}(\omega)$ approaches the following limits for the different values of the viscosity ν :

$$\lim_{\nu \rightarrow 0} \gamma^{(1,2)}(\omega) = \frac{\ell^{(if)}}{\mu^{(if)}}, \quad (21a)$$

$$\lim_{\nu \rightarrow \infty} \gamma^{(1,2)}(\omega) = 0. \quad (21b)$$

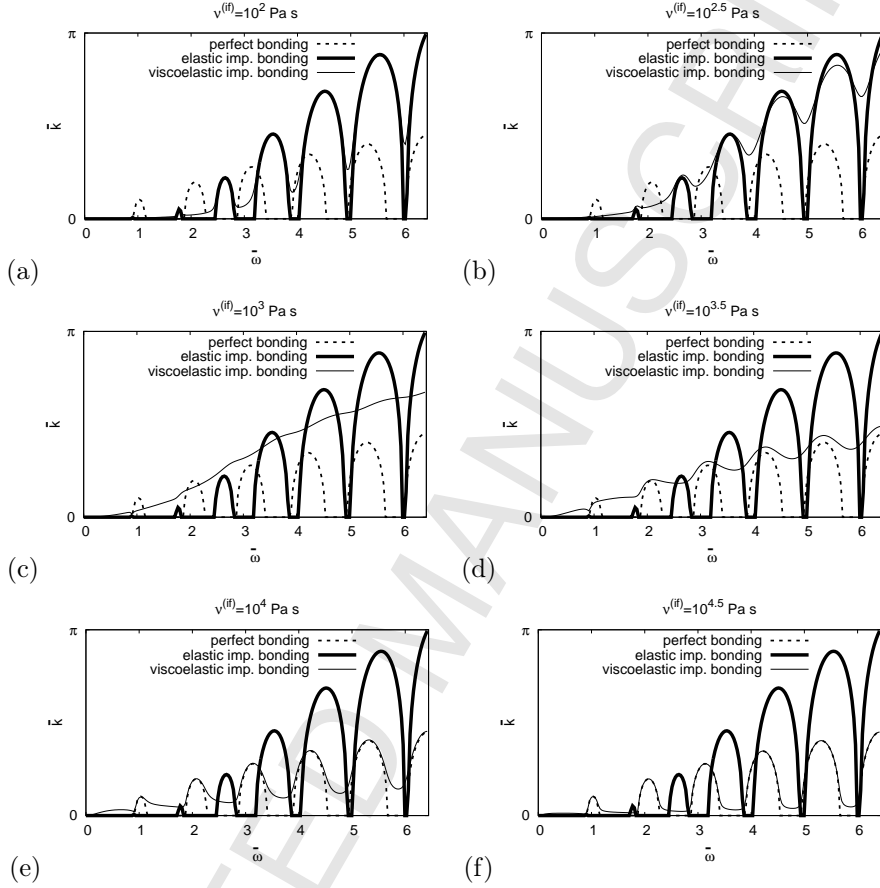


Figure 7: Attenuation coefficients for different values of the viscosity ν in the Kelvin-Voigt type of bonding model in (19) and (20).

The limit in (21a) describes the purely elastic case, and the limit in (21b) defines perfect bonding.

For this modeling layer, let us choose a small length of $\ell^{(if)} = \frac{\ell}{1000}$, and a shear modulus in complex form $\mu^{(if)} = \mu^{(if)}(\omega)$ as given by Eq. (5) for a Kelvin-Voigt material. For the real part of the shear modulus we choose $\mu_R^{(if)} = 10^7$ GPa, which is significantly smaller than the shear moduli of **both** the inclusion and the matrix. In the following, we consider the case of a purely elastic interface behavior and a viscoelastic frequency-dependent behavior of the interface. **The results are shown in Fig. 7. The case of perfect bonding is presented as a reference.**

- **Elastic imperfect bonding:** If the imaginary part of the shear modulus $\mu^{(if)}$ is equal to zero, $\mu_I^{(if)} = 0$, then the bonding model reveals a frequency-

independent and purely elastic character (see the left panel of Fig. 3). Andrianov et al. [49] have shown that with increasing values of $\gamma^{(1,2)}$ all frequency bands shift closer together, while the magnitude of the imaginary parts of the wavenumber changes. This effect can also be observed in Fig. 7 (the first peak of the stop band is at $\{\bar{\omega}, \bar{k}\} = \{0.9, 0.02\}$).

- **Viscoelastic imperfect bonding:** Let us now assume a viscoelastic and therefore complex and frequency-dependent behavior of the shear modulus $\mu^{(if)} = \mu^{(if)}(\omega)$ in Eq. (5) for a Kelvin-Voigt material. The development of the stop bands with increasing values for ν are illustrated in the different panels of Fig. 7. For relatively small values of ν , the gaps in the values for the attenuations coefficients take non-zero values, and the frequency regions for which wave propagation without a decline of the traveling signal is possible, disappear. If the viscosity takes large values $\nu \rightarrow \infty$, then one can see from (21b) that also the bonding factor $\gamma^{(1,2)}$ tends to zero, and bonding becomes perfect.

This example has shown how the quality of bonding affects the dispersion relation of the composite. By introducing elastic imperfect bonding, the dispersion characteristics of the material have changed. The then following part has shown that by introducing a time-dependent behavior in the interface the frequency bands, for which propagation of the signal is possible without attenuation, vanish due to dissipation of the kinetic energy.

4. Transmittance and reflectance of a layered composite of finite length: Transfer-matrix method

In the present section, we consider a layered composite of finite length as shown in Fig. 8, which consists of $N_1 + N_2 + 1$ unit cells. Each cell has the same

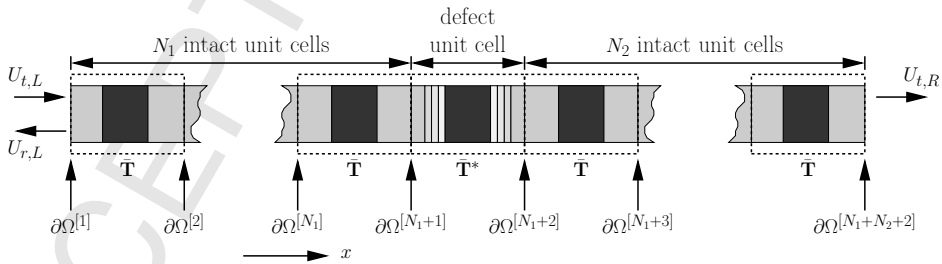


Figure 8: A layered composite material, which consists of a periodic arrangement of unit cells. The transfer-matrix for intact cells is denoted as $\bar{\mathbf{T}}$, while the transfer-matrix for defect cells is denoted as $\bar{\mathbf{T}}^*$.

length ℓ , so that the total length of the layered composite is $[N_1 + N_2 + 1]\ell$. The first N_1 cells on the left side and the last N_2 cell on the right side are intact unit cells. A single defect unit cell is located between the intact unit cells, in which the matrix has already been degraded.

Consider a shear wave in the form (15) traveling through the material. Let us introduce two displacement field vectors in the form

$$\mathbf{U}_L = \begin{bmatrix} U_{t,L} \\ U_{r,L} \end{bmatrix}, \quad \mathbf{U}_R = \begin{bmatrix} U_{t,R} \\ 0 \end{bmatrix}. \quad (22)$$

The elements of the vectors \mathbf{U}_L are the displacement of incident waves $U_{t,L}$, and the displacement of the overall reflected waves $U_{r,L}$ on the left side of the composite, as is shown in Fig. 8. In the vector \mathbf{U}_R , the element $U_{t,R}$ is the displacement of the wave, which has been transmitted through the composite. These displacement field vectors (22) are related by a global 2×2 transfer-matrix \mathbf{T} of the overall composite in the form

$$\mathbf{U}_R = \mathbf{T}\mathbf{U}_L. \quad (23)$$

In order to understand the acoustic properties of the material, let us introduce the transmittance and reflectance of the composite as follows (see Zhao [60])

$$\text{transmittance:} \quad \Phi_t = \left\| \frac{U_{t,R}}{U_{t,L}} \right\|^2 = \left\| \frac{\det(\mathbf{T})}{T_{22}} \right\|^2, \quad (24a)$$

$$\text{reflectance:} \quad \Phi_r = \left\| \frac{U_{r,L}}{U_{t,L}} \right\|^2 = \left\| \frac{T_{21}}{T_{22}} \right\|^2. \quad (24b)$$

Both the transmittance Φ_t and the reflectance Φ_r can take values ranging between zero and one. If $\Phi_t = 0$ and $\Phi_r = 1$, then the signal is completely reflected. If $\Phi_t = 1$ and $\Phi_r = 0$, then the signal completely passes through the material. For an elastic material the sum of the transmittance Φ_t and the reflectance Φ_r is equal to one, $\Phi_t + \Phi_r = 1$.

The global transfer-matrix \mathbf{T} in (23) results from the number, the arrangements, and compositions of the different unit cells in the composite. For the composite in Fig. 8, the global transfer-matrix can be expressed in terms of the different unit cell matrices as

$$\mathbf{T} = \underbrace{\bar{\mathbf{T}}\bar{\mathbf{T}} \dots \bar{\mathbf{T}}\bar{\mathbf{T}}}_{N_2 \text{ times}} \bar{\mathbf{T}}^* \underbrace{\bar{\mathbf{T}}\bar{\mathbf{T}} \dots \bar{\mathbf{T}}\bar{\mathbf{T}}}_{N_1 \text{ times}} = [\bar{\mathbf{T}}]^{N_2} \bar{\mathbf{T}}^* [\bar{\mathbf{T}}]^{N_1}, \quad (25)$$

where $\bar{\mathbf{T}}$ is the transfer-matrix for an intact unit cell, and $\bar{\mathbf{T}}^*$ is the transfer-matrix for a defect unit cell with a degraded matrix. **In Appendix C, we discuss the compositions of the unit cell transfer matrices for intact unit cells $\bar{\mathbf{T}}$ and for defect unit cells $\bar{\mathbf{T}}^*$ in detail.**

In the following examples we illustrate the numerical examples, in which the transfer-matrix method is applied to study wave propagation in layered composites for an arrangement with intact unit cells and for the case, in which one defect unit cell is located in the structure.

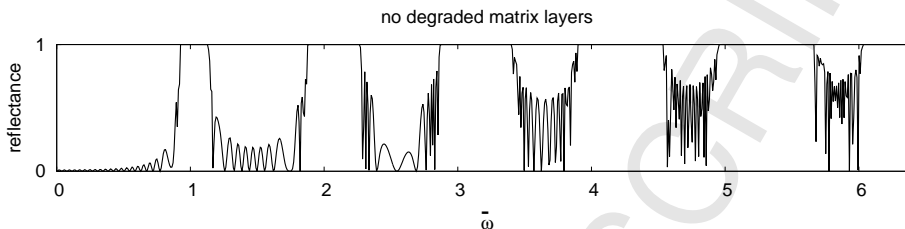


Figure 9: Reflectance for layered composite with 100 intact unit cells.

4.1. Numerical examples: Reflectance for a layered composite with intact unit cells

Figure 9 illustrates the reflectance of a layered material of 100 intact unit cells (see the case "lin 0" in Tab. 1), which consist of the same materials as in the numerical example in Sect. 3.1. Bonding between the different layers and unit cells is taken to be perfect. A similar problem has been studied in Fig. 5 (a) by the Floquet-Bloch approach for an infinite number of intact unit cells. Let us compare the physical meanings of the reflectance and the attenuation factor k_I of the wavenumber: for values larger than 0, both the reflectance and k_I define a frequency region, in which the propagating signal will attenuate. Comparing the results from Figs. 9 and 5 (a), we find that the frequency bands for which the traveling signal attenuates in Fig. 5 (a) are in a similar region as the frequency bands, for which the reflectance in Fig. 9 becomes equal to zero.

4.2. Numerical examples: a defect unit cell in a finite layered composite

Consider a layered composite, which is composed of eleven unit cells. These unit cells are composed of an aluminum inclusion and a polymer matrix, as described in Sect. 3.1. As in the previous examples, we apply the material parameters of aluminum (shear modulus $\mu^{(1)} = 26$ GPa, mass density $\rho^{(1)} = 2700$ kg/m³) for the inclusions, and for the matrix we apply the material parameters of poly-lactic acid (PLA) (shear modulus $\mu^{(10)} = 1.287$ GPa, mass density $\rho^{(10)} = 1251.5$ kg/m³ [58]). In the following we study the transmittance of the finite layered material in two brief examples: In the first example we consider a single defect unit cell with a linearly degraded matrix as described by (17a), and we consider different locations of such a cell in the layered material. In the second part, we assume that the defect unit cell is located in the center of the composite, and contrast the different transmittance bands for the three degradation modes in Eqs. (17), which are illustrated in Fig. 4.

4.2.1. Linear matrix degradation

Figure 10 (a) shows the transmittance of the considered material, when all eleven unit cells are intact with properties from "lin 0" in Table 1. In the panels (b)-(d) we assume that ten unit cells are intact, while a single unit cell has a degraded matrix with properties that are described by "lin 5" in Table 1.

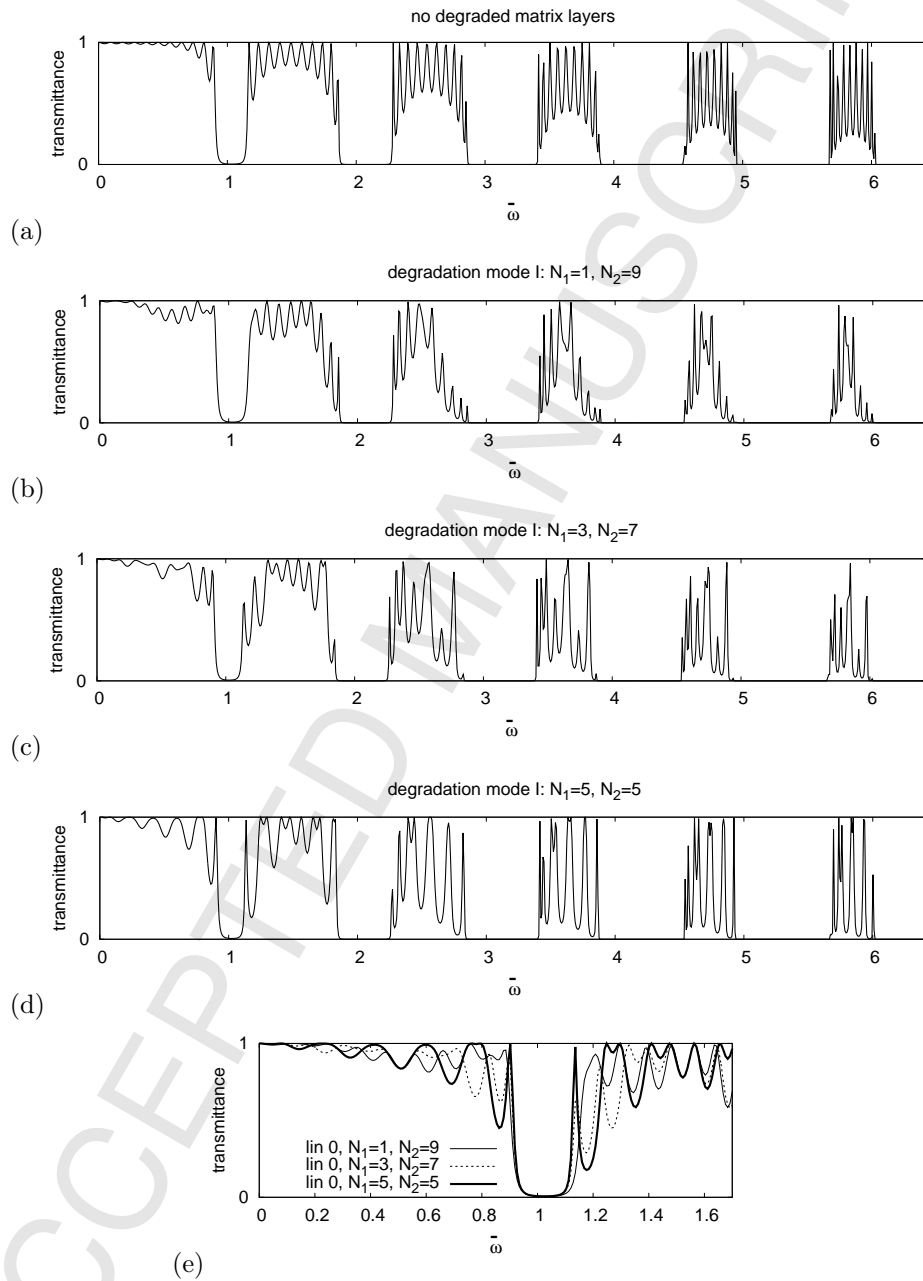


Figure 10: Transmittance of a layered composite with 11 unit cells.

In the different panels we consider different locations for the defect unit cell:
In panel (b) the second unit cell is defect; in panel (c) the fourth unit cell is

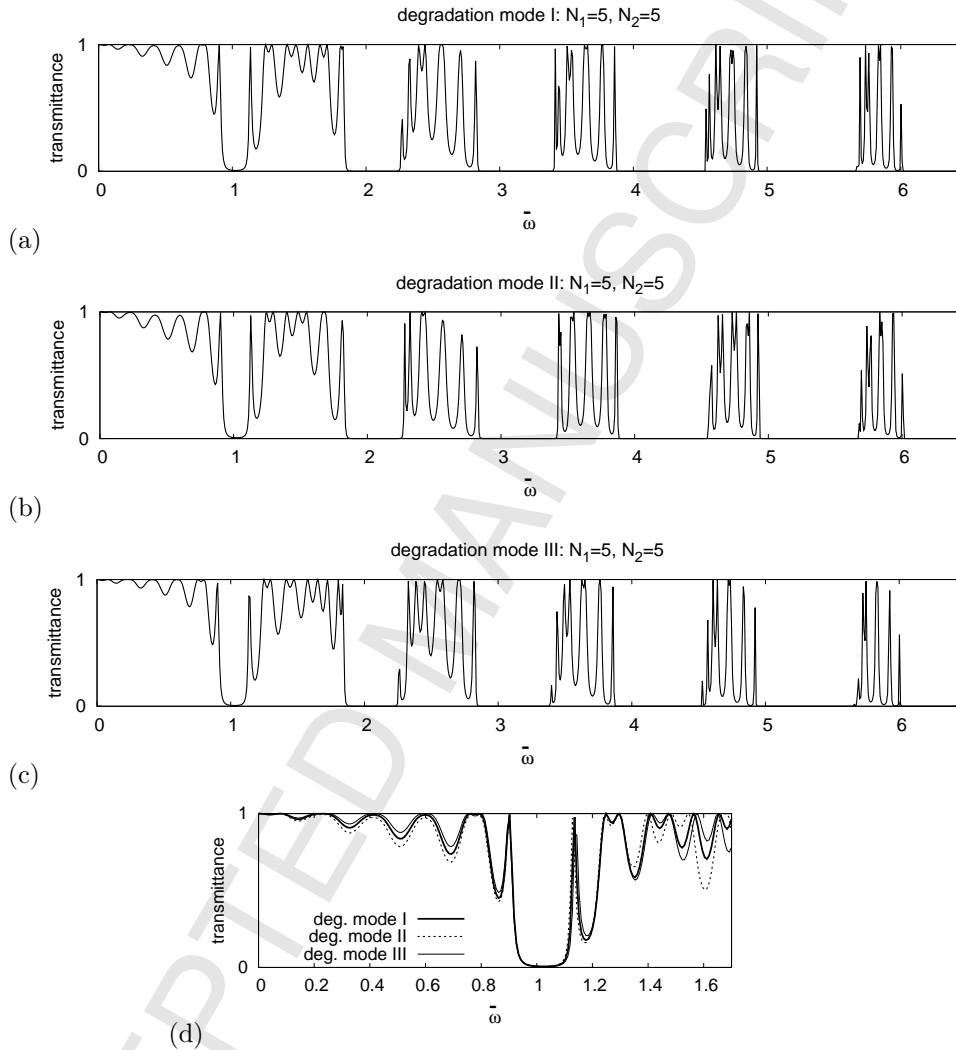


Figure 11: Transmittance bands of eleven unit cells, of which ten unit cells are intact, and a defect unit cell, which is located in the center of the composite.

defect; in panel (d) the sixth or central unit cell is defect. Creating a symmetric problem by exchanging the values for N_1 and N_2 , we obtain the same results for the transmittance. The different panels (b)-(d) show that the location of the defect unit cell affects the composite's formation of the transmittance. The results in (b)-(d) are relatively close together, because just a single unit cell in the composite is subjected to degradation. In order to illustrate the differences in the results, the enlarged view in Fig. 10 (e) contrasts the results for the transmittance frequencies from panels (b)-(d) on the scale $0 \leq \bar{\omega} \leq 1.7$.

The results show that analyzing the transmittance bands for a certain frequency range allows identifying the location of a degraded unit cell in a layered material. Analogously to our discussion in Section 3.1.2, the transmittance proves valuable information, which can be used to draw conclusions on the composition of microstructure. We refer to Hussein et al. [59] to give an example for a work, in which the authors derive the composition of a finite layered material for a known dispersion relation.

4.2.2. Three different degradation modes

In the previous paragraph we contrasted the transmittance of a layered composite for different locations of a defect unit cell, and we assumed a linear degradation of the matrix in this defect unit cell. Let us now again consider a finite layered composite of eleven unit cells, in which ten unit cells are intact, and a defect unit cell is located in the center of the composite. Figure 11 contrasts the results for the transmittance for the three degradation modes, which have been presented in Tab. 2 in Sect. 3.1. Panel (a) is for the degradation mode I, panel (b) for the degradation mode II, and panel (c) is for the degradation mode III. Also in this example, the results for transmittance are relatively close together. In order to illustrate the differences in the results Fig. 11 (d) contrasts the results for the transmittance frequencies from panels (a)-(c) on the scale $0 \leq \bar{\omega} \leq 1.7$. The local extrema of the curves in panel (d) have approximately the same location, while the magnitudes of the extrema differ. The curves for degradation mode II have the lowest local minima, and the curves for degradation mode III have the highest minima.

The different panels in Fig. 11 illustrate that the transmittance of the material changes with the mode of degradation of the matrix. The present example illustrates that not only the location of a defect unit cell can be identified, but also the degradation mode.

5. Effective mechanical properties: asymptotic homogenization method

Wave propagation through such a layered composite as shown in Fig. 1 has been treated exactly by the application of the Floquet-Bloch approach in Sect. 3. Many engineering applications require the analysis of two-dimensional and three-dimensional structures, such as fiber-reinforced composites. The numerical treatment of composites with a heterogeneous microstructure might be time consuming, especially if the characteristic length of the heterogeneities is much smaller than the macroscopic problem under consideration. A solution to this problem is replacing the original heterogeneous problem by a modeling material with the same macroscopic or homogenized mechanical properties. A popular method to achieve this goal is the asymptotic homogenization method. This approach is described in detail in the book by Panasenko [31], and it has been applied in different research works, for example in order to study wave propagation in periodic media by Andrianov et al. [32], Craster et al. [35, 36], and by Antonakakis & Craster [37], and to study heat transfer in composites [57, 61].

In this approach we assume that the macroscopic size L of the problem under investigation is much larger than the typical size of the heterogeneities ℓ . These lengths are related by a *small parameter* ε via $L = \varepsilon^{-1}\ell$. The original coordinate variable x is replaced by a slow coordinate variable η , which measures the displacement on the macroscopic scale. A second coordinate ζ denoted as the fast coordinate variable is introduced, which measures the displacement within the unit cell (see Appendix D.1). Such splitting of the variables in order to obtain homogenized wave equations of different orders is described in detail by Bensoussan et al. [30]. Comparing the results of the asymptotic homogenization method to the exact results of the Floquet-Bloch approach for a relatively simple problem such a layered composite allows estimating the error of the asymptotic homogenization method before the asymptotic approach is applied to study problems with more complex geometries. This strategy shows that an efficient analysis of composites can be achieved by combining the merits or different approaches (also see the discussion on this topic by Andrianov et al. [39]).

We now consider the layered composite in Fig. 1. The displacement $u_{\pm}^{(n)}$ of the component $\Omega_{\pm}^{(n)}$ is then also presented in the form of an asymptotic expansion in terms of the small parameter ε ,

$$u_{\pm}^{(n)} = u_{0,\pm}^{(n)} + \varepsilon u_{1,\pm}^{(n)} + \varepsilon^2 u_{2,\pm}^{(n)} + \dots = \sum_{j=0} \varepsilon^j u_{j,\pm}^{(n)}, \quad (26)$$

where the first term $u_0 = u_0(\eta, t) = u_{0,\pm}^{(n)}(\eta, t)$ is the homogenized term, which depends on the slow coordinate variable η and time t , and the then following terms $u_{j,\pm}^{(n)} = u_{j,\pm}^{(n)}(\eta, \zeta, t)$ with $j = 1, 2, \dots$ are correction terms of the asymptotic order ε^j , which depend on both the slow and fast coordinate variables η and ζ , respectively, and on time t . Due to the L -periodicity of the layers in terms of ζ , the correction terms $u_{j,\pm}^{(n)}$ have the same periodicity with respect to L ,

$$u_{j,\pm}^{(n)}(\eta, \zeta, t) = u_{j,\pm}^{(n)}(\eta, \zeta + L, t), \quad j = 1, 2, 3, \dots \quad (27)$$

This periodicity allows us to investigate the macroscopic problem on the micro-scale within a single unit cell of the material. This herein considered unit cell presents a symmetric problem, for which the boundary conditions in the center and on the outer boundaries of the unit cell can be replaced by (see Bakhvalov & Panasenko [62])

$$u_{j,\pm}^{(n)} \Big|_{x=0} = 0, \quad (28a)$$

$$u_{j,\pm}^{(n)} \Big|_{x=\pm \frac{L}{2}} = 0. \quad (28b)$$

After substitution of the asymptotic expansion of the displacement (26) into wave Eq. (1) and applying the derivatives in (D.2), we obtain a recurrent system

of wave equations of different asymptotic orders in the form

$$\mu^{(n)} \left[\frac{\partial^2 u_{j-2,\pm}^{(n)}}{\partial \eta^2} + 2 \frac{\partial^2 u_{j-1,\pm}^{(n)}}{\partial \eta \partial \zeta} + \frac{\partial^2 u_{j,\pm}^{(n)}}{\partial \zeta^2} \right] = \rho^{(n)} \frac{\partial u_{j-2,\pm}^{(n)}}{\partial t}, \quad (29)$$

where all terms $u_{-1,\pm}^{(n)}$ and $u_{-2,\pm}^{(n)}$ are equal to zero.

Equations (2) describe the conditions for perfect contact at the interfaces $\partial\Omega_{\pm}^{(n,n+1)}$, where $n = 1, 2, \dots, N-1$, which in terms of both the slow and fast coordinate variables become

$$u_{j,\pm}^{(n)} \Big|_{\partial\Omega_{\pm}^{(n,n+1)}} = u_{j,\pm}^{(n+1)} \Big|_{\partial\Omega_{\pm}^{(n,n+1)}}, \quad (30a)$$

$$\mu^{(n)} \left[\frac{\partial u_{j-1,\pm}^{(n)}}{\partial \eta} + \frac{\partial u_{j,\pm}^{(n)}}{\partial \zeta} \right]_{\partial\Omega_{\pm}^{(n,n+1)}} = \mu^{(n+1)} \left[\frac{\partial u_{j-1,\pm}^{(n+1)}}{\partial \eta} + \frac{\partial u_{j,\pm}^{(n+1)}}{\partial \zeta} \right]_{\partial\Omega_{\pm}^{(n,n+1)}} \quad (30b)$$

Equations (3) describe the conditions for imperfect contact at the interface $\partial\Omega^{(1,2)}$, which in terms of both the slow and fast coordinate variables become

$$\pm \varepsilon \left[u_{j,\pm}^{(2)} - u_{j,\pm}^{(1)} \right]_{\partial\Omega^{(1,2)}} = \gamma^{(1,2)} \mu^{(1)} \left[\frac{\partial u_{j-1,\pm}^{(1)}}{\partial \eta} + \frac{\partial u_{j,\pm}^{(1)}}{\partial \zeta} \right]_{\partial\Omega^{(1,2)}} \quad (31a)$$

$$\mu^{(1)} \left[\frac{\partial u_{j-1,\pm}^{(1)}}{\partial \eta} + \frac{\partial u_{j,\pm}^{(1)}}{\partial \zeta} \right]_{\partial\Omega_{\pm}^{(1,2)}} = \mu^{(2)} \left[\frac{\partial u_{j-1,\pm}^{(2)}}{\partial \eta} + \frac{\partial u_{j,\pm}^{(2)}}{\partial \zeta} \right]_{\partial\Omega_{\pm}^{(1,2)}}. \quad (31b)$$

This set of equations in (29) - (31) is valid if the different material parameters are of the same asymptotic order, $\mu^{(a)} \sim \mu^{(b)}$ and $\rho^{(a)} \sim \rho^{(b)}$, where $a = 1, 2, \dots, N$ and $b = 1, 2, \dots, N$. Non-local effects, which result from large differences in the values for the material parameters, are discussed in detail by Cherednichenko et al. [63] and Gałka et al. [61]. **The details on the procedure to obtain the homogenized wave equations of different asymptotic orders are given in Appendix D.3.**

From the recurrent system of **wave equations** and boundary conditions of different asymptotic orders we obtain the homogenized wave equation of the asymptotic order ε^{P-1} as

$$\left[\sum_{p=1}^P \langle \mu \rangle_{p-1} \varepsilon^{p-1} \frac{\partial^{p+1} u_0}{\partial \eta^{p+1}} \right] + \mathcal{O}(\varepsilon^P) = \langle \rho \rangle \frac{\partial^2 u_0}{\partial t^2}, \quad (32)$$

where $\langle \mu \rangle_{p-1}$ are the ε^{p-1} order effective shear moduli, and $\langle \rho \rangle$ is the effective mass density.

If we consider a harmonic wave with the amplitude U_0 in the form

$$u_0(\eta, t) = U_0 \exp(ik\eta) \exp(i\omega t) \quad (33)$$

and substitute (33) into (32), then we obtain the dispersion relation in the form

$$\left[\sum_{p=1}^P \langle \mu \rangle_{p-1} [ik]^{p+1} \varepsilon^{p-1} \right] + \mathcal{O}(\varepsilon^P) = -\omega^2 \langle \rho \rangle. \quad (34)$$

This equation (34) allows us to determine the approximation of dispersion relation in the homogenized material.

5.1. Comparison of the results obtained by the asymptotic homogenization method to exact results obtained by the Floquet-Bloch approach

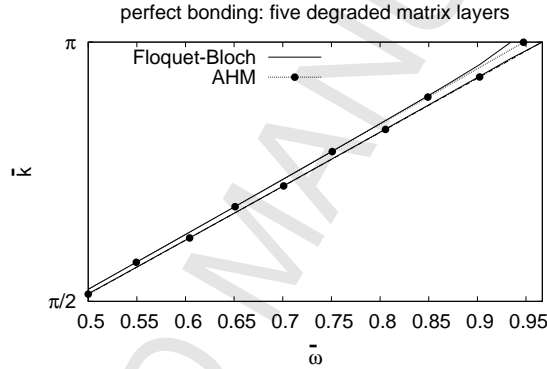


Figure 12: The results for the first branch of the pass band for both the asymptotic homogenization method and the Floquet-Bloch approach (see Sect. 3.1, Table 2).

In the present example we compare the results for the frequency band structure, which have been obtained by the AHM, to the exact results, which have been obtained by the Floquet-Bloch approach.

For the ε^2 order approximation, Eqs. (32) and (34) become

$$\langle \mu \rangle_0 \frac{\partial^2 u_0}{\partial \eta^2} + \langle \mu \rangle_2 \varepsilon^2 \frac{\partial^4 u_0}{\partial \eta^4} + \mathcal{O}(\varepsilon^3) = \langle \rho \rangle \frac{\partial^2 u_0}{\partial t^2}, \quad (35a)$$

$$-\langle \mu \rangle_0 k^2 + \langle \mu \rangle_2 k^4 \varepsilon^2 + \mathcal{O}(\varepsilon^3) = -\omega^2 \langle \rho \rangle. \quad (35b)$$

Note that in (35) the ε^1 order modulus $\langle \mu \rangle_1$ is equal to zero. Some authors such as Metrikine [64] mentioned that parabolic equations such as (35a) break the causality. Hui & Oskay [65] show that we can organize the homogenization procedure in such a way that we will obtain hyperbolic equations. Nevertheless, because we only deal with the lower part of the frequency spectrum, the local inertia term is sufficient for us.

Let us now consider a unit cell, in which the matrix has degraded with degradation mode I and II, as illustrated in Sect. 3.1 in Table 2. The results for the first branch of the pass band for both the asymptotic homogenization

method and the Floquet-Bloch approach are contrasted in Fig. 12. The upper curves in a certain line style are for degradation mode II, and the lower ones for degradation mode I. Because the curves for both the degradation modes are relatively close together, we enlarged the top parts of the curves. We can see that both the solutions for the asymptotic homogenization method and for the Floquet-Bloch approach are relatively close together.

6. Discussion of the Results

This article studies wave propagation in a layered material, in which bonding between the inclusion phase and the degradable matrix is considered to be imperfect, which might be the result of a production error, a crack, or corrosion [66]. If due to such an imperfection the matrix is subjected to environmental influences such as moisture, then the matrix might degrade, for example if biodegradable polymers are chosen for the matrix constituent. This degraded part of the matrix is modeled in terms of different layers with decreased values of the mechanical properties. A similar approach has been applied by Wu et al. [8] to model functionally graded materials. In order to model bonding between the inclusion and the matrix, we applied the spring-layer model, and a modification of this model to take viscoelastic behavior into account. An alternative approach to model imperfect bonding was to introduce an artificial interphase layer with geometric and mechanical properties that define the bonding quality.

We apply different techniques in order to identify the changes of the mechanical properties of the composite with the degradation process of the matrix, and with changes in the bonding characteristics between the matrix and the inclusion. The Floquet-Bloch approach gives exact results for the pass and stop bands in the case of layered materials with a periodic microstructure. Although the analysis of layered composites by the Floquet-Bloch approach is of limited practical value, these exact results might provide useful references for approaches, in which the dispersion relation is approximated by semi-analytical or numerical methods, for example by the finite difference method, the plane-wave expansion method, or by the asymptotic homogenization methods.

In the following part we applied the transfer-matrix method in order to study a layered composite of a finite number of unit cells. In different numerical studies we considered a single defect unit cell with a degraded matrix, and we have shown that the degradation progress as well as the location of the defect unit cell can be identified by the analysis of the transmittance of the composite.

The asymptotic homogenization method has been applied to analyze the impact of the matrix degradation and bonding quality on the effective or macroscopic properties of the material. The results for the dispersion relation obtained by the asymptotic homogenization method have been compared to the exact results, which have been previously obtained by the Floquet-Bloch approach.

In the framework of this article, material parameters from the literature have been applied. For the matrix degradation three different degradation modes have been studied and the resulting dispersion relation has been contrasted.

Experiments on layered composites at different stages of the degradation of the matrix might be helpful to study the accuracy of the herein obtained results.

ACCEPTED MANUSCRIPT

Appendix A. Imperfect bonding between the layers: spring-layer model

In order to derive the conditions, which describe imperfect bonding between the constituents, let us introduce a thin artificial modeling layer $\Omega^{(if)}$ with a thickness $\ell^{(if)}$, a constant shear modulus $\mu^{(if)}$, and a constant mass density $\rho^{(if)}$ between the two layers $\Omega^{(1)}$ and $\Omega^{(2)}$, as it is shown in Fig. A.13. The mechanical properties of this model layer shall define the bonding quality between $\Omega^{(1)}$ and $\Omega^{(2)}$. The wave equation of this model layer has the form

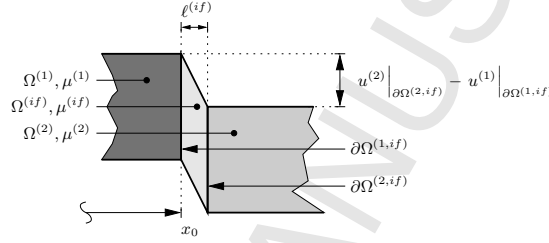


Figure A.13: Imperfect bonding at the interface $\partial\Omega^{(1,2)}$ between the constituents $\Omega^{(1)}$ and $\Omega^{(2)}$ is simulated by an interphase material $\Omega^{(if)}$ of small thickness, $\ell^{(if)} \rightarrow 0$.

$$\mu^{(if)} \frac{\partial^2 u^{(if)}}{\partial x^2} = \rho^{(if)} \frac{\partial^2 u^{(if)}}{\partial t^2}, \quad (\text{A.1})$$

where $\mu^{(if)}$ is the shear modulus, $\rho^{(if)}$ is the mass density, and $u^{(if)} = u^{(if)}(x, t)$ is the displacement of the interphase layer. The thickness $\ell^{(if)}$ is assumed to be small, $\ell^{(if)} \ll \ell^{(n)}$, so that we can take

$$\left| \mu^{(if)} \frac{\partial^2 u^{(if)}}{\partial x^2} \right| \gg \left| \rho^{(if)} \frac{\partial^2 u^{(if)}}{\partial t^2} \right|. \quad (\text{A.2})$$

Then wave Eq. (A.1) can be written as

$$\mu^{(if)} \frac{\partial^2 u^{(if)}}{\partial x^2} \approx 0 \quad \Leftrightarrow \quad u^{(if)} = \alpha^{(if)} + \beta^{(if)} x. \quad (\text{A.3})$$

In Eq. (A.3), $\alpha^{(if)}$ and $\beta^{(if)}$ are two integration constants, which have to be determined from the conjugate conditions between $\Omega^{(1)}$ and $\Omega^{(if)}$ at their common interface $\partial\Omega^{(1,if)}$ and between $\Omega^{(2)}$ and $\Omega^{(if)}$ at their common interface $\partial\Omega^{(2,if)}$. We take bonding between the interfaces $\partial\Omega^{(1,if)}$ and $\partial\Omega^{(2,if)}$ to be perfect, so that both the displacements and the shear stresses between the two

constituents at these interfaces are equal:

$$u^{(1)} \Big|_{\partial\Omega^{(1,if)}} = u^{(if)} \Big|_{\partial\Omega^{(1,if)}}, \quad (\text{A.4a})$$

$$\mu^{(1)} \frac{\partial u^{(1)}}{\partial x} \Big|_{\partial\Omega^{(1,if)}} = \mu^{(if)} \frac{\partial u^{(if)}}{\partial x} \Big|_{\partial\Omega^{(1,if)}}, \quad (\text{A.4b})$$

$$u^{(2)} \Big|_{\partial\Omega^{(2,if)}} = u^{(if)} \Big|_{\partial\Omega^{(2,if)}}, \quad (\text{A.4c})$$

$$\mu^{(2)} \frac{\partial u^{(2)}}{\partial x} \Big|_{\partial\Omega^{(2,if)}} = \mu^{(if)} \frac{\partial u^{(if)}}{\partial x} \Big|_{\partial\Omega^{(2,if)}}. \quad (\text{A.4d})$$

From the conjugate conditions (A.4a) and (A.4c), which demand equal displacements at the interfaces $\partial\Omega^{(1,if)}$ and $\partial\Omega^{(2,if)}$, we can determine the constants $\alpha^{(if)}$ and $\beta^{(if)}$ in (A.3):

$$\alpha^{(if)} = u^{(1)} \Big|_{\partial\Omega^{(1,if)}} - \frac{x_0}{\ell^{(if)}} \left[u^{(2)} \Big|_{\partial\Omega^{(2,if)}} - u^{(1)} \Big|_{\partial\Omega^{(1,if)}} \right], \quad (\text{A.5a})$$

$$\beta^{(if)} = \frac{1}{\ell^{(if)}} \left[u^{(2)} \Big|_{\partial\Omega^{(2,if)}} - u^{(1)} \Big|_{\partial\Omega^{(1,if)}} \right]. \quad (\text{A.5b})$$

If we substitute (A.5) into (A.3) and apply the conjugate condition (A.4b), we obtain the following condition, which describes the differences in the displacements of the layers $\Omega^{(1)}$ and $\Omega^{(2)}$ at the interfaces of $\Omega^{(if)}$:

$$u^{(2)} \Big|_{\partial\Omega^{(2,if)}} - u^{(1)} \Big|_{\partial\Omega^{(1,if)}} = \mu^{(1)} \frac{\partial u^{(1)}}{\partial x} \Big|_{\partial\Omega^{(1,2)}} \frac{\ell^{(if)}}{\mu^{(if)}}. \quad (\text{A.6})$$

The ratio of $\ell^{(if)}$ to $\mu^{(if)}$ defines the bonding factor $\gamma^{(1,2)}$ in (4).

Appendix B. Comments on the Floquet-Bloch approach

The system of equation, which result from the boundary conditions in (2) for perfect bonding and (3) for imperfect bonding within the unit cell and from the boundary conditions (16) for the outer boundaries of the unit cell, can be written in the form

$$\mathbf{M} \cdot \mathbf{U} = \mathbf{0}, \quad (\text{B.1})$$

where \mathbf{U} is the vector of all terms $U_{1,\pm}^{(n)}$ and $U_{2,\pm}^{(n)}$ in the displacement function (15), and $\mathbf{0}$ is a zero vector of the same size as \mathbf{U} :

$$\mathbf{U} = \begin{pmatrix} U_{1,-}^{(N)} \\ U_{2,-}^{(N)} \\ U_{1,-}^{(N-1)} \\ U_{2,-}^{(N-1)} \\ \dots \\ U_{1,-}^{(2)} \\ U_{2,-}^{(2)} \\ U_{1,-}^{(1)} \\ U_{2,-}^{(1)} \\ U_{1,+}^{(2)} \\ U_{2,+}^{(2)} \\ \dots \\ U_{1,+}^{(N-1)} \\ U_{2,+}^{(N-1)} \\ U_{1,+}^{(N)} \\ U_{2,+}^{(N)} \end{pmatrix}, \quad \mathbf{0} = \begin{pmatrix} 0 \\ 0 \\ 0 \\ 0 \\ \dots \\ 0 \\ 0 \\ 0 \\ 0 \\ 0 \\ 0 \\ \dots \\ 0 \\ 0 \\ 0 \\ 0 \end{pmatrix}. \quad (\text{B.2})$$

In (B.1), the elements of the quadratic $(2N-1) \times (2N-1)$ matrix \mathbf{M} result from the factors of the terms $U_{1,\pm}^{(n)}$ and $U_{2,\pm}^{(n)}$ in (2), (3) and (16). The determinant $\det(\mathbf{M}) = 0$ gives the dispersion relation, which relates the frequency of the propagation signal to the wavenumber.

Appendix C. Comments on the transfer-matrix approach

Appendix C.1. Intact unit cell

Let us first consider an intact unit cell, as shown in the top part of Fig. 4, which consists of an inclusion and a matrix. The transfer matrices $\mathbf{t}^{(1)}$ and $\mathbf{t}^{(2)}$ for each of the homogeneous inclusion layer $\Omega^{(1)}$ and the matrix layers $\Omega_{\pm}^{(2)}$, respectively, then become

$$\mathbf{t}^{(1)} = \begin{bmatrix} \exp(ik\ell^{(1)}) & 0 \\ 0 & \exp(-ik\ell^{(1)}) \end{bmatrix} \quad \text{for } \Omega^{(1)}, \quad (\text{C.1a})$$

$$\mathbf{t}^{(2)} = \begin{bmatrix} \exp(ik\frac{\hat{\ell}^{(2)}}{2}) & 0 \\ 0 & \exp(-ik\frac{\hat{\ell}^{(2)}}{2}) \end{bmatrix} \quad \text{for } \Omega_{\pm}^{(2)}. \quad (\text{C.1b})$$

For the interfaces $\partial\Omega^{(1,2)}$ between the inclusion and the matrix, the transfer-matrix becomes

$$\mathbf{T}^{(1,2)} = \begin{bmatrix} T_{11}^{(1,2)} & T_{12}^{(1,2)} \\ T_{21}^{(1,2)} & T_{22}^{(1,2)} \end{bmatrix} \quad \text{for } \partial\Omega_+^{(1,2)}, \quad (\text{C.2a})$$

$$\mathbf{T}^{(2,1)} = \begin{bmatrix} T_{11}^{(2,1)} & T_{12}^{(2,1)} \\ T_{21}^{(2,1)} & T_{22}^{(2,1)} \end{bmatrix} = [\mathbf{T}^{(2,1)}]^{-1} \quad \text{for } \partial\Omega_-^{(2,1)}, \quad (\text{C.2b})$$

with the elements

$$T_{11}^{(1,2)} = T_{22}^{(1,2)} = \frac{Z^{(2)} + Z^{(1)}}{2Z^{(2)}}, \quad (\text{C.3a})$$

$$T_{12}^{(1,2)} = T_{21}^{(1,2)} = \frac{Z^{(2)} - Z^{(1)}}{2Z^{(2)}}, \quad (\text{C.3b})$$

for the transfer-matrix $\mathbf{T}^{(1,2)}$ in (C.2a). The elements for the transfer-matrix $\mathbf{T}^{(2,1)}$ in (C.2b) are determined analogously. In Eq. (C.3), $Z^{(n)} = \sqrt{\mu^{(n)}\rho^{(n)}}$ are the acoustic impedances of the components $\Omega_{\pm}^{(n)}$. Then the transfer-matrix of a single intact unit cell is obtained by combining (C.1) and (C.2) as follows,

$$\bar{\mathbf{T}} = \mathbf{t}^{(2)}\mathbf{T}^{(2,1)}\mathbf{t}^{(1)}\mathbf{T}^{(1,2)}\mathbf{t}^{(2)}\mathbf{T}^{(2,2)}, \quad (\text{C.4})$$

where $\mathbf{T}^{(2,2)} = \mathbf{I}$ is the transfer-matrix for the interfaces $\partial\Omega_{\pm}^{(N,N)}$ between the different intact unit cells. This transfer-matrix $\mathbf{T}^{(2,2)}$ is equal to the identity matrix, because all intact unit cells have the same material parameters for the matrix.

Appendix C.2. Degraded unit cell

Consider a degraded unit cell, as shown in Fig. 4, where $\Omega^{(1)}$ is the inclusion, $\Omega_{\pm}^{(N)}$ is the intact part of the matrix, and $\Omega_{\pm}^{(2)}, \Omega_{\pm}^{(3)}, \dots, \Omega_{\pm}^{(N-1)}$ are layers that model the degraded part of the matrix.

- If bonding between all the layers is taken to be perfect, then for a single unit cell with degraded matrix the transfer-matrix becomes

$$\bar{\mathbf{T}}^* = \mathbf{t}^{(N)}\mathbf{T}^{(N,N-1)} \dots \mathbf{t}^{(2)}\mathbf{T}^{(2,1)}\mathbf{t}^{(1)}\mathbf{T}^{(1,2)}\mathbf{t}^{(2)} \dots \mathbf{t}^{(N)}\mathbf{T}^{(N,2)}, \quad (\text{C.5})$$

where the different transfer matrices are determined analogously to (C.1) - (C.3). We consider the outer layers of the defect unit cells to have intact matrix material, so that $\mathbf{T}^{(N,2)} = \mathbf{I}$.

- In the case of imperfect bonding between the inclusion and the matrix, we introduce an additional thin artificial layer (superscript "if") between the inclusion $\Omega^{(1)}$ and the neighboring matrix layers $\Omega_{\pm}^{(2)}$, so that the unit cell transfer-matrix becomes

$$\begin{aligned} \bar{\mathbf{T}}^* = & \mathbf{t}^{(N)}\mathbf{T}^{(N,N-1)} \dots \\ & \mathbf{t}^{(2)}\mathbf{T}^{(2,if)}\mathbf{t}^{(if)}\mathbf{T}^{(if,1)}\mathbf{t}^{(1)}\mathbf{T}^{(1,if)}\mathbf{t}^{(if)}\mathbf{T}^{(if,2)}\mathbf{t}^{(2)} \dots \\ & \mathbf{t}^{(N)}\mathbf{T}^{(N,2)}. \end{aligned} \quad (\text{C.6})$$

There exist different techniques to simulate imperfect bonding between two constituents in a composite. The herein applied method to introduce an artificial layer has been discussed in [49], and compared to the spring-layer model, which has been introduced in Sect. 2.2.

Appendix D. Comments on the asymptotic homogenization method

Appendix D.1. Replacement of the original coordinate variable x by the slow and fast coordinate variables η and ζ , respectively

In the asymptotic homogenization approach, the original coordinate variable x is replaced by the slow and fast coordinate variables η and ζ , respectively. These coordinate variables are related via

$$x \rightarrow \eta, \quad \zeta = \varepsilon^{-1}\eta. \quad (\text{D.1})$$

Consequently, the total lengths of the constituent $\Omega_{\pm}^{(n)}$ remains $\ell^{(n)}$ in terms of the slow coordinate variable η , while in terms of the fast coordinate variable these lengths change to $L^{(n)}$, where $L^{(n)} = \varepsilon^{-1}\ell^{(n)}$ (see Fig. D.14). The deriva-

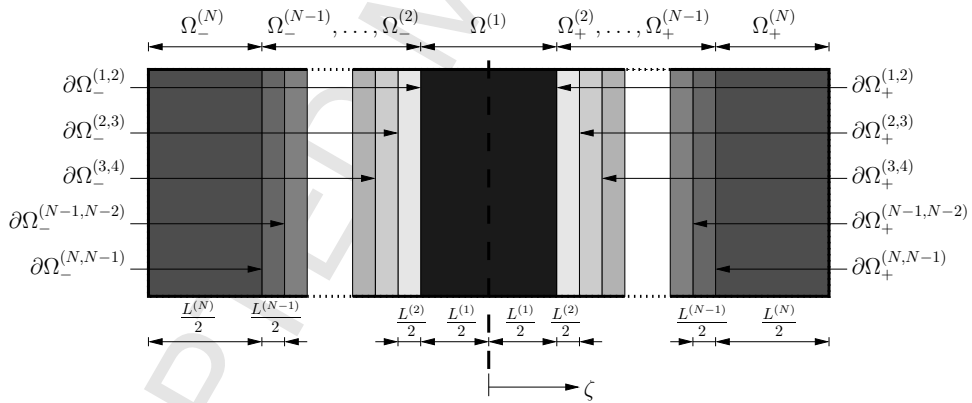


Figure D.14: The periodically repeated unit cell in Fig. 2 in terms of the fast coordinate variable ζ .

tives with respect to x are rewritten in terms of the fast and slow coordinate variables,

$$\frac{\partial}{\partial x} \rightarrow \frac{\partial}{\partial \eta} + \frac{1}{\varepsilon} \frac{\partial}{\partial \zeta}, \quad \frac{\partial^2}{\partial x^2} \rightarrow \frac{\partial^2}{\partial \eta^2} + \frac{2}{\varepsilon} \frac{\partial}{\partial \eta} \frac{\partial}{\partial \zeta} + \frac{1}{\varepsilon^2} \frac{\partial^2}{\partial \zeta^2}. \quad (\text{D.2})$$

Appendix D.2. Correction terms of the displacement $u_{j,\pm}^{(n)}$

From wave equation (29) we obtain the following system of wave equations after substituting $j = 1, 2, 3$,

$$\mu^{(n)} \left[\frac{\partial^2 u_{-1,\pm}^{(n)}}{\partial \eta^2} + 2 \frac{\partial^2 u_{0,\pm}^{(n)}}{\partial \eta \partial \zeta} + \frac{\partial^2 u_{1,\pm}^{(n)}}{\partial \zeta^2} \right] = \rho^{(n)} \frac{\partial^2 u_{-1,\pm}^{(n)}}{\partial t^2}, \quad (\text{D.3a})$$

$$\mu^{(n)} \left[\frac{\partial^2 u_{0,\pm}^{(n)}}{\partial \eta^2} + 2 \frac{\partial^2 u_{1,\pm}^{(n)}}{\partial \eta \partial \zeta} + \frac{\partial^2 u_{2,\pm}^{(n)}}{\partial \zeta^2} \right] = \rho^{(n)} \frac{\partial^2 u_{0,\pm}^{(n)}}{\partial t^2}. \quad (\text{D.3b})$$

In (D.3a), some terms can be canceled out immediately, because $u_{-1,\pm}^{(n)} = 0$, and because the homogenized term $u_{0,\pm} = u_0$ is independent from ζ . These equations (D.3) allow us to determine the different order correction terms of the displacements $u_j^{(n)}(\eta, \zeta, t)$:

- Substituting $j = 1$ into (D.3a), we obtain

$$\frac{\partial^2 u_1^{(n)}}{\partial \zeta^2} = 0, \quad (\text{D.4a})$$

$$\Leftrightarrow \frac{\partial u_1^{(n)}}{\partial \zeta} = \beta_1^{(n)} \frac{\partial u_0}{\partial \eta}, \quad (\text{D.4b})$$

$$\Leftrightarrow u_1^{(n)} = \left[\alpha_1^{(n)} + \beta_1^{(n)} \zeta \right] \frac{\partial u_0}{\partial \eta}, \quad (\text{D.4c})$$

where $\alpha_1^{(n)}$ and $\beta_1^{(n)}$ are N sets of integration constants.

- Substituting $j = 2$ into (D.3b), we obtain

$$\frac{\partial^2 u_2^{(n)}}{\partial \zeta^2} = \frac{\rho^{(n)}}{\mu^{(n)}} \frac{\partial^2 u_0}{\partial t^2} - \left[1 + 2\beta_1^{(n)} \right] \frac{\partial^2 u_0}{\partial \eta^2} \quad (\text{D.5a})$$

$$= \left[\frac{\langle \mu \rangle_0 \rho^{(n)}}{\langle \rho \rangle \mu^{(n)}} - 1 - 2\beta_1^{(n)} \right] \frac{\partial^2 u_0}{\partial \eta^2}, \quad (\text{D.5b})$$

$$\Leftrightarrow \frac{\partial^2 u_2^{(n)}}{\partial \zeta^2} = \left[\beta_2^{(n)} + \left(\frac{\langle \mu \rangle_0 \rho^{(n)}}{\langle \rho \rangle \mu^{(n)}} - 1 - 2\beta_1^{(n)} \right) \zeta \right] \frac{\partial^2 u_0}{\partial \eta^2}, \quad (\text{D.5c})$$

$$\Leftrightarrow u_2^{(n)} = \left[\alpha_2^{(n)} + \beta_2^{(n)} \zeta + \left(\frac{\langle \mu \rangle_0 \rho^{(n)}}{\langle \rho \rangle \mu^{(n)}} - 1 \right. \right. \quad (\text{D.5d})$$

$$\left. \left. - 2\beta_1^{(n)} \right) \frac{\zeta^2}{2} \right] \frac{\partial^2 u_0}{\partial \eta^2}, \quad (\text{D.5e})$$

where $\alpha_2^{(n)}$ and $\beta_2^{(n)}$ are N sets of integration constants.

Appendix D.3. Homogenized wave equation of different asymptotic orders

The homogenized wave equations of different asymptotic orders can be obtained by the following steps:

- Equation (29) allows us to obtain the ansatzes for the different order correction terms of the displacements $u_1^{(n)}, u_2^{(n)}, \dots$, in (26). The integration constants in these ansatzes are determined from (28), which demands zero displacement in the center and at the outer faces of the unit cell, and from (30) and (31) at the different interfaces $\partial\Omega_{\pm}^{(n,n+1)}$. The details on these ansatzes are presented in Appendix D.2.
- Once the differences in the displacements have been determined, the homogenization operator

$$\frac{1}{L} \int_{-\frac{L}{2}}^{\frac{L}{2}} \dots d\zeta \quad (\text{D.6})$$

is applied to both the left and the right side of wave Eq. (29) in order to obtain the effective shear moduli $\langle\mu\rangle_j$ of the order $\mathcal{O}(\epsilon^j)$ as well as the effective mass density $\langle\rho\rangle$. Applying the operator (D.6) to the wave Eq. (29) then leads to

$$\begin{aligned} & \frac{1}{L} \left\{ \sum_{n=1}^N \int_{\Omega^{(n)}} \mu^{(n)} \left[\frac{\partial^2 u_{j,\pm}^{(n)}}{\partial\eta\partial\zeta} + \frac{\partial^2 u_{j-1,\pm}^{(n)}}{\partial\eta^2} \right] d\zeta \right\} \\ &= \frac{1}{L} \left[\sum_{n=1}^N \int_{\Omega^{(n)}} \rho^{(n)} \frac{\partial^2 u_{j-1,\pm}^{(n)}}{\partial t^2} \right]. \end{aligned} \quad (\text{D.7})$$

Note that in arrival to (D.7), we have applied

$$\sum_{n=1}^N \int_{\Omega^{(n)}} \frac{\partial^2 u_{j+1,\pm}^{(n)}}{\partial\eta^2} + \frac{\partial^2 u_{j,\pm}^{(n)}}{\partial\eta\partial\zeta} d\zeta = 0. \quad (\text{D.8})$$

The herein described procedure has been applied in different studies to obtain the effective material properties of composites.

Acknowledgements

The authors are grateful to the anonymous reviewers for their valuable comments and suggestions, which helped to improve the paper. This work was supported by a Qatar University Internal Grant (QUUG-CAM-CAM-15/16-3) for H. Topol. This work has received funding from the European Union's Horizon 2020 research and innovation program under the Marie Skłodowska-Curie grant agreement no. 655177 for V.V. Danishevskyy.

References

- [1] W. J. Parnell, Effective wave propagation in a prestressed nonlinear elastic composite bar, *IMA J. Appl. Math.* 72 (2007) 223–244.
- [2] P. Zhang, W. J. Parnell, Soft phononic crystals with deformation-independent band gaps, *Proc. R. Soc. A* 473 (2017) 20160865.
- [3] L. Avérous, E. Pollet, Biodegradable polymers, in: L. Avérous, E. Pollet (Eds.), *Environmental Silicate Nano-Biocomposites*, Springer, 2012.
- [4] B. D. Ulery, L. S. Nair, C. T. Laurencin, Biomedical applications of biodegradable polymers, *J. Polym. Sci. B Polym. Phys.* 49 (2011) 832–864.
- [5] H. Topol, H. Demirkoparan, T. J. Pence, A. S. Wineman, Time-evolving collagen-like structural fibers in soft tissues: Biaxial loading and spherical inflation, *Mech. Time-Depend. Mat.* 12 (2017) 1–29.
- [6] U. Icardi, S. Locatto, A. Longo, Assessment of recent theories for predicting failure of composite laminates, *Appl. Mech. Rev.* 60 (2007) 76–86.
- [7] M. Safaei, A. Sheidaei, M. Baniassadi, S. Ahzi, M. Mosavi Mashhadi, F. Pourboghra, An interfacial debonding-induced damage model for graphite nanoplatelet polymer composites, *Comput. Mater. Sci.* 96 (2015) 191–199.
- [8] M.-L. Wu, L.-Y. Wu, W.-P. Yang, L.-W. Chen, Elastic wave band gaps of one-dimensional phononic crystals with functionally graded materials, *Smart Mater. Struct.* 18 (2009) 115013.
- [9] M. V. Golub, S. I. Fomenko, T. Q. Bui, C. Zhang, Y.-S. Wang, Transmission and band gaps of elastic sh waves in functionally graded periodic laminates, *Int. J. Solids Struct.* 49 (2012) 344–354.
- [10] S. I. Fomenko, M. V. Golub, C. Zhang, T. Q. Bui, Y.-S. Wang, In-plane elastic wave propagation and band-gaps in layered functionally graded phononic crystals, *Int. J. Solids Struct.* 51 (2014) 2491–2503.
- [11] R. K. Burla, A. V. Kumar, B. V. Sankar, Implicit boundary method for determination of effective properties of composite microstructures, *Int. J. Solids Struct.* 46 (2009) 2514–2526.
- [12] G. Floquet, Sur les équations différentielles linéaires à coefficients périodiques, *Ann. Sci. l'École Norm. Sup.* 12 (1883) 47–88.
- [13] F. Bloch, Über die Quantenmechanik der Elektronen in Kristallgittern, *Z. Phys.* 52 (1928) 555–600.
- [14] M. Ruzzene, A. Baz, Control of wave propagation in periodic composite rods using shape memory inserts, *J. Vib. Acoust.* 122 (2000) 151–159.

- [15] N. A. Shul'ga, Propagation of elastic waves in periodically inhomogeneous media, *Int. Appl. Mech.* 39 (2003) 763–796.
- [16] M. Shen, W. Cao, Acoustic bandgap formation in a periodic structure with multilayer unit cells, *J. Phys. D: Appl. Phys.* 33 (2000) 1150–1154.
- [17] J. Virieux, SH-wave propagation in heterogeneous media : Velocity-stress finite-difference method, *Geophysics* 49 (1984) 1933–1957.
- [18] J. Virieux, P-SV wave propagation in heterogeneous media : Velocity-stress finite-difference method, *Geophysics* 51 (1986) 889–901.
- [19] M. S. Kushwaha, Stop-bands for periodic metallic rods: sculptures that can filter noise, *Appl. Phys. Lett.* 70 (1997) 3218–3220.
- [20] Y. Cao, Z. Hou, Y. Liu, Convergence problem of plane-wave expansion method for phononic crystals, *Phys. Lett. A* 327 (2004) 247–253.
- [21] E. G. Barnwell, W. J. Parnell, I. D. Abrahams, Antiplane elastic wave propagation in pre-stressed periodic structures; tuning, band gap switching and invariance, *Wave Motion* 63 (2016) 98–110.
- [22] Z. Liu, C. T. Chan, P. Sheng, A. L. Goertzen, J. H. Page, Elastic wave scattering by periodic structures of spherical objects: theory and experiment, *Phys. Rev. B* 62 (2000) 2446–2457.
- [23] I. E. Psarobas, N. Stefanou, A. Modinos, Scattering of elastic waves by periodic arrays of spherical bodies, *Phys. Rev. B* 62 (2000) 278–291.
- [24] L. Rayleigh, On the influence of obstacles arranged in rectangular order upon the properties of a medium, *Phil. Mag.* 34 (1892) 481–502.
- [25] V. V. Zalipaev, A. B. Movchan, C. G. Poulton, R. C. McPhedran, Elastic waves and homogenization in oblique periodic structures, *Proc. R. Soc. A* 458 (2002) 1887–1912.
- [26] V. Filonova, A. Fafalis, J. Fish, Dispersive computational continua, *Comput. Methods Appl. Mech. Engrg.* 298 (2016) 58–79.
- [27] W. Cao, W. Qi, Plane wave propagation in finite 2–2 composites, *J. Appl. Phys.* 78 (1995) 4627–4632.
- [28] L. Wang, S. I. Rokhlin, Stable reformulation of transfer matrix method for wave propagation in layered anisotropic media, *Ultrasonics* 39 (2001) 413–424.
- [29] A.-L. Chen, Y.-S. Wang, Study on band gaps of elastic waves propagating in one-dimensional disordered phononic crystals, *Physica B* 392 (2007) 369–378.

- [30] A. Bensoussan, J.-L. Lions, G. Papanicolaou, *Asymptotic Analysis for Periodic Structures*, North-Holland, 1978.
- [31] G. Panasenko, *Multi-scale Modelling for Structures and Composites*, Springer, 2005.
- [32] I. V. Andrianov, V. I. Bolshakov, V. V. Danishevs'kyi, D. Weichert, Higher order asymptotic homogenization and wave propagation in periodic composite materials, *Proc. R. Soc. A* 464 (2008) 1181–1201.
- [33] I. V. Andrianov, V. V. Danishevs'kyi, D. Weichert, Simple estimation on effective transport properties of a random composite material with cylindrical fibres, *Z. angew. Math. Phys.* 59 (2008) 889–903.
- [34] W. J. Parnell, I. D. Abrahams, Dynamic homogenization in periodic fibre reinforced media. quasi-static limit for sh waves, *Wave Motion* 43 (2006) 474–498.
- [35] R. V. Craster, J. Kaplunov, J. Postnova, High-frequency asymptotics, homogenisation and localisation for lattices, *Q. J. Mech. Appl. Math.* 63 (2010) 497–519.
- [36] R. V. Craster, J. Kaplunov, A. V. Pichugin, High-frequency homogenization for periodic media, *Proc. Roy. Soc. A* 466 (2010) 2341–2362.
- [37] T. Antonakakis, R. V. Craster, High-frequency asymptotics for microstructured thin elastic plates and platonics, *Proc. Roy. Soc. A* 468 (2012) 1408–1427.
- [38] I. V. Andrianov, V. V. Danishevs'kyi, H. Topol, D. Weichert, Homogenization of a 1D nonlinear dynamical problem for periodic composites, *Z. angew. Math. Mech.* 91 (2011) 523–534.
- [39] I. V. Andrianov, J. Awrejcewicz, V. V. Danishevs'kyi, D. Weichert, Wave propagation in periodic composites: Higher-order asymptotic analysis versus plane-wave expansions method, *J. Comput. Nonlinear Dynam.* 6 (2011) 011015 (8 pages).
- [40] A. L. Kalamkarov, I. V. Andrianov, V. V. Danishevs'kyi, Asymptotic homogenization of composite materials and structures, *Appl. Mech. Rev.* 62 (2009) 030802 (20 pages).
- [41] M. Goland, E. Reissner, The stresses in cemented joints, *J. Appl. Mech.* 11 (1944) 17–27.
- [42] I. V. Andrianov, V. I. Bolshakov, V. V. Danishevs'kyi, D. Weichert, Asymptotic simulation of imperfect bonding in periodic fibre-reinforced composite materials under axial shear, *Int. J. Mech. Sci.* 49 (2007) 1344–1354.

- [43] G. Geymonat, F. Krasucki, S. Lenci, Mathematical analysis of a bonded joint with a soft thin adhesive, *Math. Mech. Solids* 4 (1999) 201–225.
- [44] F. Krasucki, S. Lenci, Analysis of interfaces of variable stiffness, *Int. J. Solids Struct.* 37 (2000) 3619–3632.
- [45] Z. Hashin, Thin interphase/imperfect interface in elasticity with application to coated fiber composites, *J. Mech. Phys. Solids* 50 (2002) 2509–2537.
- [46] J. M. Vivar-Pérez, U. Gabbert, H. Berger, R. Rodríguez-Ramos, J. Bravo-Castillero, R. Guinovart-Díaz, F. J. Sabina, A dispersive nonlocal model for wave propagation in periodic composites, *J. Mech. Mater. Struct.* 51 (1986) 889–901.
- [47] M. Gosz, B. Moran, J. D. Achenbach, Effect of a viscoelastic interface on the transverse behavior of fiber-reinforced composites, *Int. J. Solids Struct.* 27 (1991) 1757–1771.
- [48] V. M. Sadovskii, E. P. Chentsov, Analysis of oscillation processes in a blocky medium by means of continuous models, *AIP Conf. Proc.* 1773 (2016) 080003–1 – 080003–9.
- [49] I. V. Andrianov, V. V. Danishevskyy, H. Topol, G. Rogerson, Propagation of Floquet-Bloch shear waves in viscoelastic composites: analysis and comparison of interface/interphase models for imperfect bonding, *Acta Mech.* 228 (2016) 1177–1196.
- [50] Y. Liu, D. Yu, H. Zhao, J. Wen, X. Wen, Theoretical study of two-dimensional phononic crystals with viscoelasticity based on fractional derivative models, *Phys. Lett. A* 41 (2008) 065503.
- [51] W. Wang, J. Yua, Z. Tang, General dispersion and dissipation relations in a one-dimensional viscoelastic lattice, *Phys. Lett. A* 373 (2008) 5–8.
- [52] P. L. Kapitza, The study of heat transfer in helium II, *J. Phys. (USSR)* 4 (1941) 181–210.
- [53] A. J. Levi, Z. Dong, Effective transverse response of fiber composites with nonlinear interface, *J. Mech. Phys. Solids* 46 (1998) 1279–1300.
- [54] A. J. Levi, The fiber composite with nonlinear interface - Part I: Axial tension, *J. Appl. Mech.* 67 (2000) 727–732.
- [55] V. V. Danishevskyy, J. D. Kaplunov, G. A. Rogerson, Anti-plane shear waves in a fibre-reinforced composite with a non-linear imperfect interface, *Int. J. Nonlinear Mech.* 76 (2015) 223–232.
- [56] I. V. Andrianov, V. I. Bolshakov, V. V. Danishevskyy, D. Weichert, Asymptotic study of imperfect interfaces in conduction through a granular composite material, *Proc. R. Soc. A* 466 (2010) 2707–2725.

- [57] I. V. Andrianov, H. Topol, V. V. Danishevskyy, Asymptotic analysis of heat transfer in composite materials with nonlinear thermal properties, *Int. J. Heat Mass Tran.* 111 (2017) 736–754.
- [58] M. Jamshidian, E. A. Tehrany, M. Imran, M. Jacquot, S. Desobry, Polylactic acid: Production, applications, nanocomposites, and release studies, *Compr. Rev. Food Sci. F.* 9 (2010) 552–571.
- [59] M. I. Hussein, K. Hamza, G. M. Hulbert, R. A. Scott, K. Saitou, Multiobjective evolutionary optimization of periodic layered materials for desired wave dispersion characteristics, *Struct. Multidisc. Optim.* 31 (2006) 60–75.
- [60] D. Zhao, Y. Shen, X. Zhang, X. Zhu, L. Yi, Bound states in one-dimensional acoustic parity-time-symmetric lattices for perfect sensing, *Phys. Rev. Lett.* A 380 (2016) 2698–2702.
- [61] A. Gałka, J. J. Telega, S. Tokarzewski, Heat equation with temperature-dependent conductivity coefficients and macroscopic properties of microheterogeneous media, *Math. Comput. Model.* 33 (2001) 927–942.
- [62] N. S. Bakhvalov, G. P. Panasenko, *Homogenization: Averaging Processes in Periodic Media: Mathematical Problems in the Mechanics of Composite Material*, Kluwer Academic, 1989.
- [63] K. D. Cherednichenko, V. P. Smyshlyaev, V. V. Zhikov, Non-local homogenized limits for composite media with highly anisotropic periodic fibres, *Proc. R. Soc. Edin. A* 136 (2006) 87–114.
- [64] A. V. Metrikine, On causality of the gradient elasticity models, *J. Sound Vib.* 297 (2006) 727–742.
- [65] T. Hui, C. Oskay, A comparison of homogenization and standard mechanics analyses for periodic porous composites, *Int. J. Solids Struct.* 50 (2013) 38–48.
- [66] A. Bilotta, E. Turco, Numerical sensitivity analysis of corrosion detection, *Math. Mech. Solids* 22 (2017) 72–88.